Thermal Behavior of Al and In Impurities Doped in ZnO Studied by Means of Perturbed Angular Correlation Spectroscopy

Thermal Behavior of Al and In Impurities Doped in ZnO Studied by Means of Perturbed Angular Correlation Spectroscopy

Graduate School of Natural Science & Technology

Kanazawa University

January, 2015

Submitted by Sayaka Komatsuda

(ID: 1223132001)

Certified by Wataru Sato

(Chief Adviser, Associate Professor)

ACKNOWLEDGEMENTS

Throughout the course of this study, I have received generous support from many people. Taking this opportunity, I would like to express my gratitude to the people.

I owe my deepest gratitude to Associate Professor Wataru Sato of Kanazawa University for his penetrating and constructive advice. He sincerely encouraged me in the research and his continuous support has been a great help for me. Without his encouragement, this dissertation would not have been accomplished.

I'm cordially grateful to Professor Yositaka Ohkubo of Kyoto University for his experimental support in the visiting Researchers Program and constructive suggestions for paper submissions.

I would like to express my gratitude to Professor Yoshio Kobayashi of The University of Electro-Communications for providing experimental instrument for PAC measurements.

I received generous support from Professor Satoshi Kawata of Fukuoka University for XRD measurements. I received generous support from him.

I would like to thank Professor Tetsuaki Nishida and Mr. Isao Furumoto of Kinki University for the instruction of electric conductivity measurements.

I wish to acknowledge valuable discussion with Professor Yasuhiro Yamada of Tokyo University of Science, Professor Akihiko Yokoyama and Professor Motohiro Mizuno of Kanazawa University. I appreciate continuing interest and comments on this study from them.

I'm grateful to Associate Professor Hiroki Okudera of Kanazawa University for his kind help in XRD measrements.

Advice and comments given by Junichi Kikuchi of Kanazawa University Technical Support Center has been a great help in designing experimental devices of PAC measurements.

I express my gratitude to all members of Kanazawa University Radiochemistry Laboratory for their support in everyday life.

Finally, I thank my parents, Nagao and Hisako Komatsuda, my sister, Mikako Komatsuda, for countinuous support and encouragement.

ABSTRACT

Defect-induced properties of zinc oxide (ZnO) have been attracting much attention toward their application to functional materials in a wide field of industry. Especially, physical properties brought about by Al ions and/or oxygen vacancies in ZnO are one of the most intriguing topics for the development of future electronic devices. Extrinsic-semiconductor devices such as of Al-doped ZnO are expected to be in use under various ambient conditions; the states of being of impurity ions in the matrix are susceptible to change depending on the condition. For a practical use of Al-doped ZnO device, therefore, it is important to study the stability of Al impurities and/or oxygen vacancies under various conditions. The time-differential perturbed angular correlation method (TDPAC) is very suited for that purpose because it can directly provide atomic-level information of impurity atoms.

In this study, TDPAC measurements with the $^{111}\mathrm{In}(\rightarrow{}^{111}\mathrm{Cd})$ probe were performed for Al-doped ZnO heat-treated under various conditions to examine the following dependences on the formation of local structures of Al ions: concentration of Al ions, their diffusion temperature, and ambient atmosphere. It was suggested from the experiments that thermal behaviors of the impurities are closely correlated with the concentration of atmospheric oxygen to which the samples are exposed; (1)

in air, Al impurities locally associate with each other to form minute $ZnAl_2O_4$ grains even at extremely dilute concentration of 0.01 ppm, and the $^{111}In(\rightarrow^{111}Cd)$ probe ions of about 100 ppt are trapped in the field of Al ion(s), but (2) *in vacuum*, the bound state of ^{111}In and Al formed in air dissociates by heat treatment at 1000 K, resulting in substitution of ^{111}In ions at defect-free tetrahedral Zn sites. Detailed investigation of the thermal behavior of the impurities has revealed that the dissociation reaction is triggered by the formation of oxygen vacancies in the vicinity of the locally-associated In-Al structures.

In order to extend quantitative discussion on the correlation between the thermal behavior of the impurities and the concentration of atmospheric oxygen, isothermal annealing of ZnO doped with Al and ^{111}In was performed in vacuum. TDPAC experiments have revealed that the relevant dissociation process is controlled by the first-order rate law. In addition, the activation energy E_a for the reaction was successfully evaluated from the temperature variation of the rate constants k to be 0.72(6) eV. The proposed dissociation mechanism of the impurities evidently suggests that this E_a is related to the formation energy of oxygen vacancies in Al-doped ZnO sample, which is supported by good agreement with the corresponding theoretical values (0.85 and 1.0 eV).

CONTENTS

PART II

Formation Process of Oxygen Vacancy in Zinc Oxide

INTRODUCTION

1 Practical Application of ZnO

Zinc oxide (ZnO) is a compound having a wurtzite-type crystal structure composed of zinc and oxygen as shown in Fig. 1. This compound is generally produced by burning zinc metal in air or by thermal decomposition of zinc sulfide (ZnS) or zinc nitrate ($Zn(NO_3)_2$). General properties of ZnO are listed in Table 1[1-3]. The crystal structures shared by ZnO are wurtzite, zinc blende, and rocksalt[3]. Owing to its whiteness and shielding effect for ultraviolet range, ZnO has already been applied to cosmetics, paint, medicine, and many other industrial products[4,5].

Especially, in recent years, ZnO is expected to be applied to functional devices as semiconductors because of its transparent conductivity. Due to low cost, ZnO semiconductor is also expected to substitute for indium tin oxide (ITO) which contains a rare metal indium; electric conductivity of ZnO have been discussed in numerous papers since 1960s[6-13]. As a semiconductor material, ZnO can be synthesized by various growth techniques such as hydrothermal, vapor phase, and pulse laser deposition (PLD), and magnetron sputtering[14]. In these synthesis processes, the electric properties of ZnO is variable depending on local structures (defects) formed by their heat-treatment process. It is therefore of great importance for their practical application to investigate the defect-induced properties of ZnO.

2 Semiconductor Physics of ZnO

For a practical use of ZnO as conduction-controlling device, it is of great

importance to study the relation between defects and conduction electrons. In this section, the relation between defects and the electrical properties of ZnO is described. The origin of the electric conductivity is still in controversy, but some cases are proposed as strong candidate as listed below. The Kröger-Vink notation[15] is generally used: i = interstitial site, Zn = zinc, O = oxygen, and V = vacancy. Positive excess charge is marked by a point (●), negative charge by a prime (′), and a normal cation or anion with zero effective charge by ‘‘X’’.

[a] Oxygen vacancy

Oxygen vacancies are one of the main triggers for intrinsic *n*-type electric property of ZnO. Fig. 2 is a schematic diagram of various defects. The formation of oxygen vacancies supplies one or two electronic carriers as follows:

$$V_o^X = V_o^{\bullet} + e'$$

$$V_o^{\bullet} = V_o^{\bullet\bullet} + e'$$

[b] Zinc interstitial

Zinc interstitial is also one of the main triggers that causes intrinsic *n*-type semiconductivity of ZnO. (See Fig. 2 for detail.) Zn ions migrate into more stable interstitial Zn site if the excess oxygen atoms exist in ZnO. As a result, electric carriers are supplied as shown by the following reaction:

$$Zn_i^X = Zn_i^{\bullet} + e'$$

$$Zn_i^{\bullet} = Zn_i^{\bullet\bullet} + e'$$

[c] *n*- and *p*-type impurities

ZnO doped with group 13 elements (Al, Ga, In) at substitutional Zn sites is said to exhibit *n*-type electric conductivity due to donation of conduction electrons from the impurity atoms. (See Fig. 2 for detail.) It is considered that *p*-type semiconductivity is realized by doping of univalent cations such as H^+, Ag^+, and Li^+, because holes are generated in ZnO system. However, it is quite difficult to produce *p*-type semiconductor of ZnO, compared to *n*-type doping. Because oxygen vacancies and Zn interstitials are native defects in pure ZnO, even, hole-doped ZnO exhibits *n*-type electric conductivity due to compensation of the carriers by the native defects.

3 Objective of This Work

Among the above candidates for enhancing electric conductivity, extrinsic *n*-type/*p*-type semiconductors are the most promising in terms of application to electrically controllable devices. In this work, local structures formed by impurity ions are thus their applucation studied. In general, semiconductor devices are expected to be used under various conditions. Depending on temperature and atmosphere, structural changes are likely to take place at local sites. Therefore, it is essential to study physical and chemical states of dilute impurity ions in ZnO under various conditions for the practical use of ZnO devices. Physical properties of impurity-doped ZnO are generally examined through macroscopic observations[16-20]. However, for detailed understanding of stability of impurity-doped ZnO, it is necessary to clarify thermal behaviors and interacting nature of

doped impurities by obtaining direct information at the impurity site. In such cases, radioactive probe techniques are very suited because of their high sensitivity. Taking this advantage, the time-differential perturbed angular correlation (TDPAC) method has been applied for a lot of this kind of research to investigation of local structures formed by dilute impurities and their thermal behavior in ZnO.

In the previous studies[21], local structures formed by In ions in ZnO were investigated by means of the TDPAC method with the ^{111}Cd probe formed in the disintegration of ^{111}In (denominated ^{111}In($\rightarrow^{111}$Cd) hereafter). In the same way as the In-doped ZnO, in this study, TDPAC measurements with the ^{111}In($\rightarrow^{111}$Cd) probe were performed for Al-doped ZnO heat-treated in various conditions. Among group 13 elements, Al is a ubiquitous element and is thus expected to be the most promising donor for ZnO. In addition, physical properties brought about by impurities of different metal ions such as Al and In are one of the most intriguing topics for the development of future electronic devices. From this point of view, the objective of the present study was established to study the stability of Al and ^{111}In under various conditions.

This paper consists of two parts. In PART I, the concentration dependence, the temperature dependence, and the atmosphere dependence of Al behavior were investigated under different conditions. It is suggested from a series of the above experiments that thermal behavior of the impurities is closely correlated with oxygen concentration of atmosphere to which the samples are exposed.

In PART II, in order to extend quantitative discussion on the correlation between thermal behavior of the impurities and oxygen concentration of atmosphere, in PART II, TDPAC spectra were analyzed in detail for the doped ZnO prepared under various annealing conditions, namely, isothermal and isochronal annealings in vacuum. The key

finding is that atmosphere dependence of the impurity behaviors provided a helpful clue to the kinetics of thermal behaviors of Al and ^{111}In.

4 Introduction of TDPAC Method

The TDPAC method, as well as Mössbauer spectroscopy and nuclear magnetic resonance (NMR) spectroscopy, is known as an experimental technique to obtain information on microscopic structures at the site of the probe nuclei from hyperfine interactions between the nuclear moment and extranuclear field. Unlike the NMR technique, the TDPAC method requires embedding radioisotopes as a parent of the probe, and small number of probe nuclei is available because of limited nuclearproperties. However, this method has an advantage that only a small amount of probe atoms (about 10^{10}) is required for the measurements. Furthermore, it can provide local information not only of solid but also of liquid. In the following subsection, the principle and experimental setup of the TDPAC method are explained in detail.

4-1 The $\gamma-\gamma$ Perturbed Angular Correlation

The TDPAC method provides local information at the probe site through time variation of the angular correlation of cascade γ rays, which are successively emitted in the disintegration process of the exited nuclear state of the probe atom. A typical decay scheme of a probe nucleus is shown in Fig. 3. The excited nucleus(I_i) reaches its final state(I_f) via the intermediate state(I) by emitting two γ rays with multipolarities, L_1 and

L_2. The first γ rays are isotropically emitted because the nuclei are randomly oriented in matter. Once a detector detects the first γ rays, the emission direction of the second γ rays are anisotropic; this is because the detection of the first γ rays substantially signifies the selection of a certain ensemble of oriented nuclei at the intermediate state due to the conservation of angular momentum. The second γ rays then have a directional anisotropy characterized by I_i, I, I_f, L_1, and L_2.

The angular correlation of the two γ rays, $W(\theta)$ is described as

$$W(\theta)=\sum_{k=0}^{k_{\max}} A_{kk}P_k(\cos\theta)\,, \tag{1}$$

where A_{kk} denotes the correlation coefficient representing the magnitude of the directional anisotropy, and $P_k(\cos\theta)$ is the Legendre polynomial for the k th term. (k is an even number.) The $k_{\max}$ is defined by $k_{\max}=\mathrm{Min}(2I, 2L_1, 2L_2)$ due to the conservation of angular momentum.

When there is electromagnetic interaction between probe nuclei and surrounding spins and charge distribution, nuclear precession occurs arising in time interval of the γ_1 and γ_2 emissions, and the angular correlation is perturbed. In other words, this method can provide information on the magnitude of the electric field gradient (EFG) and the magnetic hyperfine field produced at the probe nuclei through the perturbed angular correlation of γ rays. The perturbed angular correlation is described as

$$W(\theta,t)=\sum_{k=0}^{k_{\max}} A_{kk}G_{kk}(t)P_k(\cos\theta), \tag{2}$$

where $G_{22}(t)$ is the time-differential perturbation factor including all information about the perturbation at the site of the probe atoms.

When the probe nucleus has a static quadrupole interaction with an axially symmetric EFG at the probe site, $G_{kk}(t)$ is expressed as

$$G_{kk}(t) = \sum_{m,m'} \begin{pmatrix} I & I & k \\ m' & -m & m-m' \end{pmatrix}^2 \cos\left[-3(m^2-m'^2)\omega_Q t\right] . \quad (3)$$

Here, $\begin{pmatrix} I & I & k \\ m' & -m & m-m' \end{pmatrix}$ is Wigner 3-j symbol which is related with Clebsch-Gordan coefficient as follows:

$$\begin{pmatrix} j_1 & j_2 & j_3 \\ m_1 & m_2 & m_3 \end{pmatrix} = (-1)^{j_1-j_2-m_3}\left(2j_3+1\right)^{-\frac{1}{2}}\left\langle j_1 m_1 j_2 m_2 \middle| j_3 - m_3 \right\rangle . \quad (4)$$

In Eq. (3), m and m' are the magnetic quantum numbers of sublevels at the intermediate state. ω_{Q_n} is the quadrupole frequency, which is proportional to the largest component of the EFG tensor, V_{zz}, chosen as $|V_{xx}| \le |V_{yy}| \le |V_{zz}|$, and is expressed by

$$\omega_Q = -\frac{eQV_{zz}}{4I(2I-1)\hbar} , \quad (5)$$

where Q denotes the nuclear quadrupole moment, $\hbar$ is reduced Planck constant, and e is the elementary electric charge. The detailed explanation and derivation of the formula are described in Ref. 22-24.

4-2 TDPAC Technique Using ^{111}Cd Probe

In this study, the ^{111}Cd probes formed in the disintegration of different parents (^{111}In and ^{111m}Cd) were adopted. Simplified decay schemes of ^{111}In($\rightarrow{}^{111}$Cd) and ^{111m}Cd($\rightarrow{}^{111}$Cd) are shown in Fig. 4[25]. The perturbed angular correlation function is thus described hereafter for the case of the ^{111}Cd probe (nuclear state with spin I = 5/2 at the intermediate state).

Because k in Eq.(2) and Eq.(3) are even numbers, the intensity of delayed coincidence events at t and θ is approximated by the following equation:

$$W(\theta,t)=1+A_{22}G_{22}(t)P_2(\cos\theta). \tag{6}$$

According to the expression, $k_{\max}=\mathrm{Min}(2I, 2L_1, 2L_2)$ and $A_{22} \gg A_{44}$, A_{44} is negligible. Because the angular correlation depends on the values of I_i I, I_f, L_1, and L_2, A_{22}takes different values between ^{111}In and ^{111m}Cd each parent.

For the case of I = 5/2, the static perturbation function for an axially symmetric electrostatic field is deduced from Eq. (3) as

$$G_{22}(t)=\frac{1}{5}\left[1+\frac{13}{7}\cos(6\omega_Q t)+\frac{10}{7}\cos(12\omega_Q t)+\frac{5}{7}\cos(18\omega_Q t)\right]. \tag{7}$$

For γ-ray detection, in the present experiment, a conventional four-detector system was adopted, and the perturbed angular correlation as a function of the time interval between the cascade γ-ray emissions, t, is obtained by the following relation:

$$A_{22}G_{22}(t)=\frac{2[N(\pi,t)-N(\pi/2,t)]}{N(\pi,t)+2N(\pi/2,t)}. \tag{8}$$

Here, $N(\theta,t)$ ($\propto W(\theta,t)\exp(-t/\tau_N)$, where τ_N is the mean life of the intermediate state of the probe) denotes the number of the delayed coincidence events observed at an angle, θ.

4-3 Experimental Setup

Figures 5 and 6 show a block diagram and pictures of the data taking circuitry for the present TDPAC measurements. The measurement circuit consists of four BaF_2 detectors and several kinds of modules for electric signal processing. In the present work, the directional anisotropy of the angular correlations of the cascade γ rays was observed at $\pi/2$ and π directions with a conventional four-detector system. For the coincidence detection of γ rays, BaF_2 scintillators (OHYO KOKEN KOGYO/ ϕ38.1 mm $\times$ 25.4 mm) were adopted due to their excellent time resolution. For the signal processing, the circuit comprises two parts: (1) energy-information part of the cascade γ rays (SCA and SEG-428) and (2) time-information part of the time interval between the cascade γ–ray emissions (PM AMP and TAC). With respect to (1) energy- information part, detected γ rays are processed by single channel analyzers (SCA) after passing through amplifier (Amp) (Amplifier and Timing Single-Channel Analyzer 590A /SEIKO EG&G). A typical γ-ray energy spectrum of ^{111}In observed by the BaF_2 scintillators is shown in Fig. 7. The SCA discriminates γ ray energies and outputs logic signals. The output signals are sent to the router (SEG-428 /SEIKO EG&G), which judges the combination of detectors of coincidence events. As for the time-information part, the signals of cascade γ rays are received by the time-to-amplitude converter (TAC) (Time-to-Amplitude Converter 567/SEIKO EG&G) after passing through photomultiplier amplifier (12 ch PM AMP/Kaizuseisakusyo). The TAC generates an analog output

pulse proportional to the time interval of cascade γ rays. Output signals of the TAC and SEG-48 are input to the analog-to-digital converter (ADC) (ADC 4801A/Laboratory Equipment Corporation). The ADC assigns the analog signal from the TAC to each of the 1024 channels depending on their amplitude, and records the number of the delayed coincidence events at every differential time interval of γ rays. Only coincidence events signals from the TAC and SEG-48 are recorded. A typical time-dependent delayed coincidence events at the time interval of the cascade γ-ray emissions is shown in Fig. 8. Each of the eight decay curves is composed of time-differential delayed coincidence events as a function of the time interval of the cascade γ-ray detections by a set of two detectors. The present detection system records the coincidence events on four different combinations of the detector sets arranged at π radians and on the other four at $\pi/2$ radians. The ADC provides the information to the multi-channel analyzer (MCA) (MCA 48F/Laboratory Equipment Corporation) and the time spectra are displayed on monitor of a personal computer.

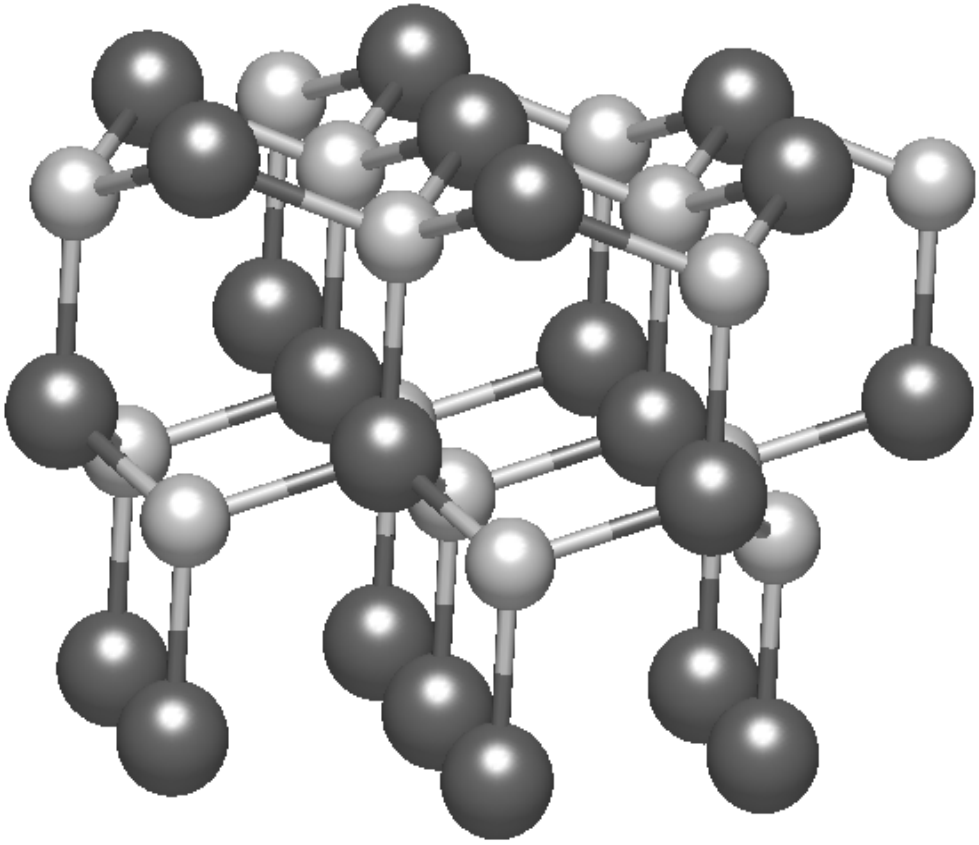

Fig. 1　Wurtzite-type crystal structure of ZnO

Table 1　Basic property of ZnO

Property	Value
Formula weight	81.37
Lattice constant	a = 3.243 Å
	b = 5.195 Å
Crystal structure	Wurtzite
Density	5.606 g/cm^3
Melting point	2273 K
Band gap	3.4 eV
Linearexpansion coefficient	a_0 = 2.008 (/℃)
	b_0 = 2.029 (/℃)
Mohs hardness	4~5

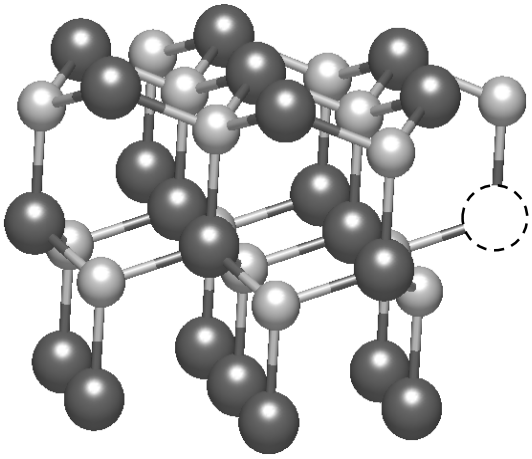

(a) Oxygen vacancy

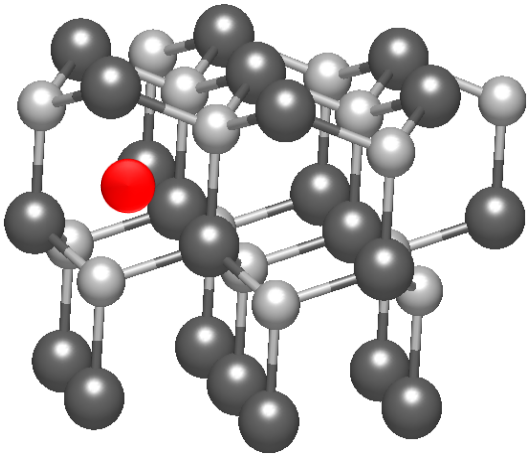

(b) Zinc interstitial

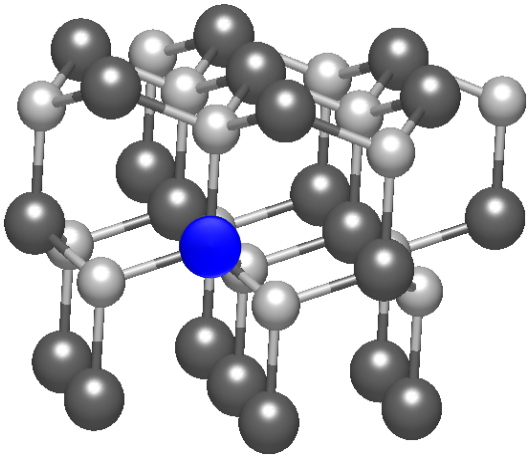

(c) Substitution of an impurity ion

Fig. 2 Wurtzite-type crystal structure of ZnO: (a) oxygen vacancy, (b) zinc interstitial, and (c) substitution of an impurity ion

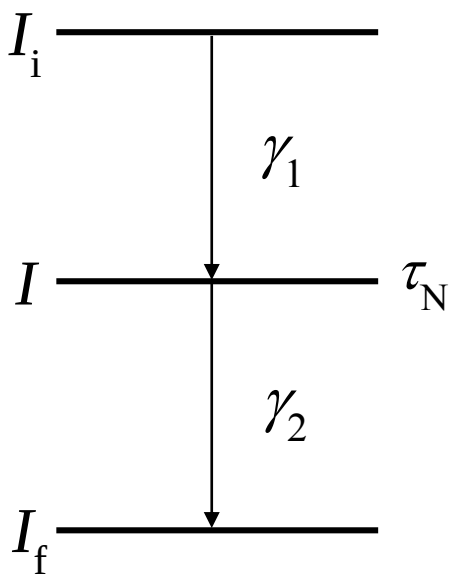

Fig. 3 Typical decay schemes of γ–γ cascade.

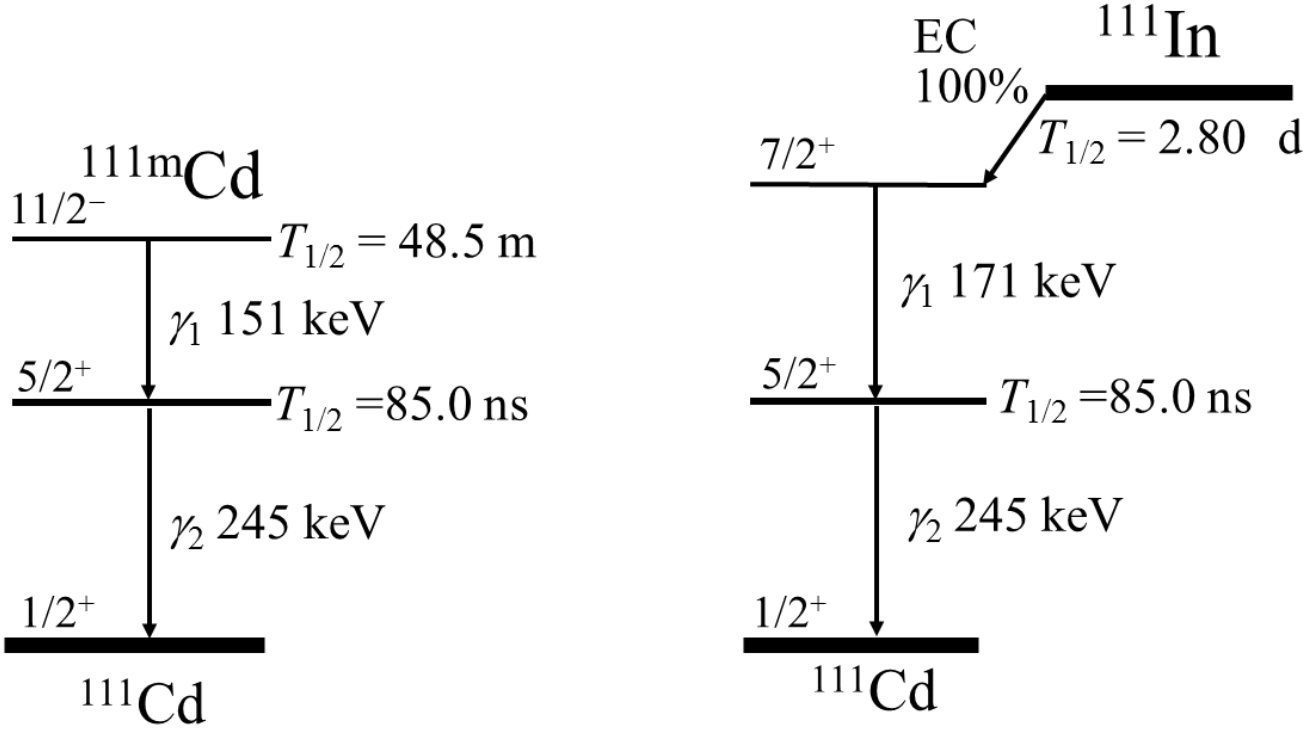

Fig. 4 Simplified decay schemes of ^{111}In($\rightarrow^{111}$Cd) and ^{111m}Cd($\rightarrow^{111}$Cd).

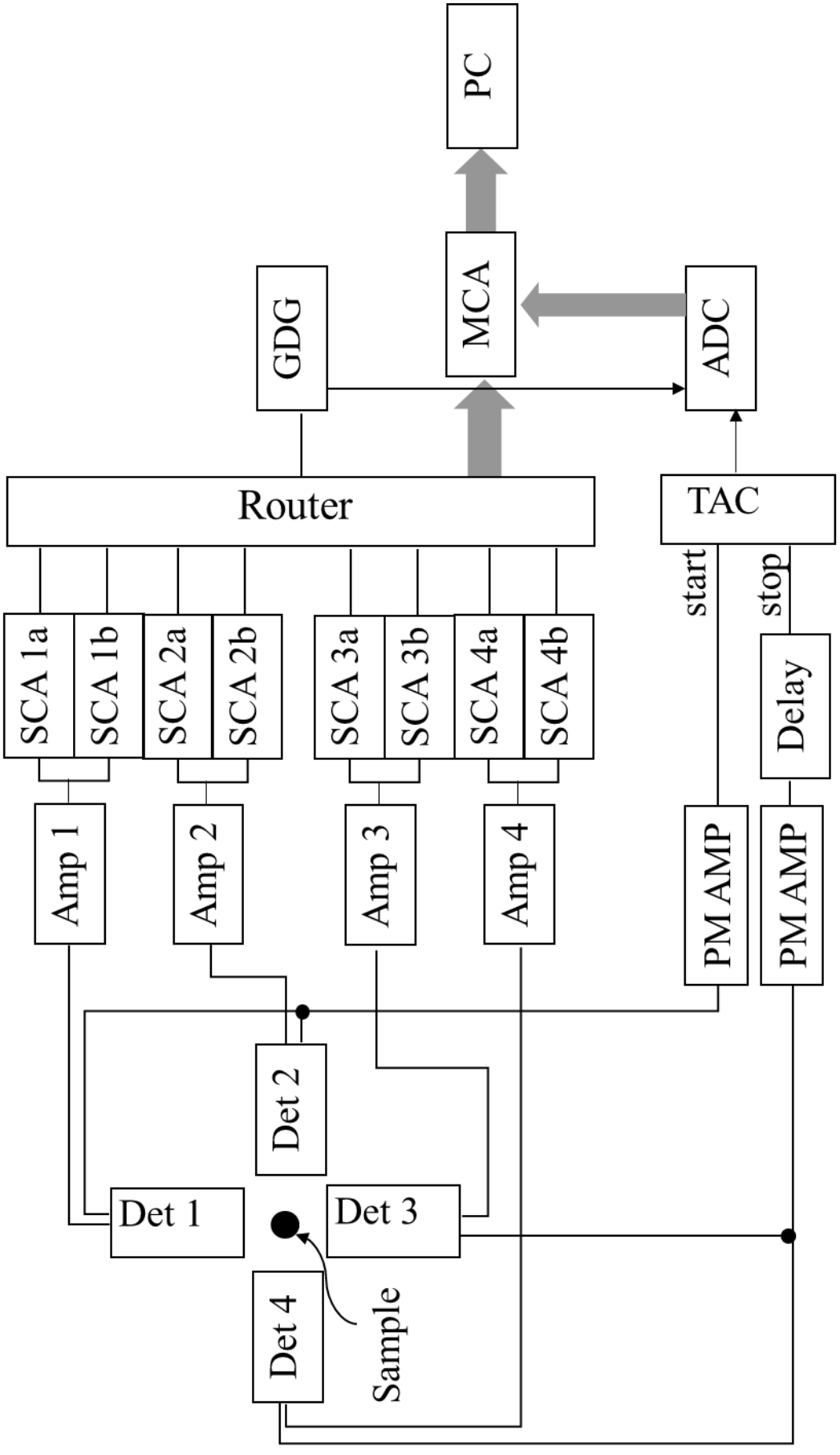

Fig. 5 Experimental apparatus for the present PAC measurements.

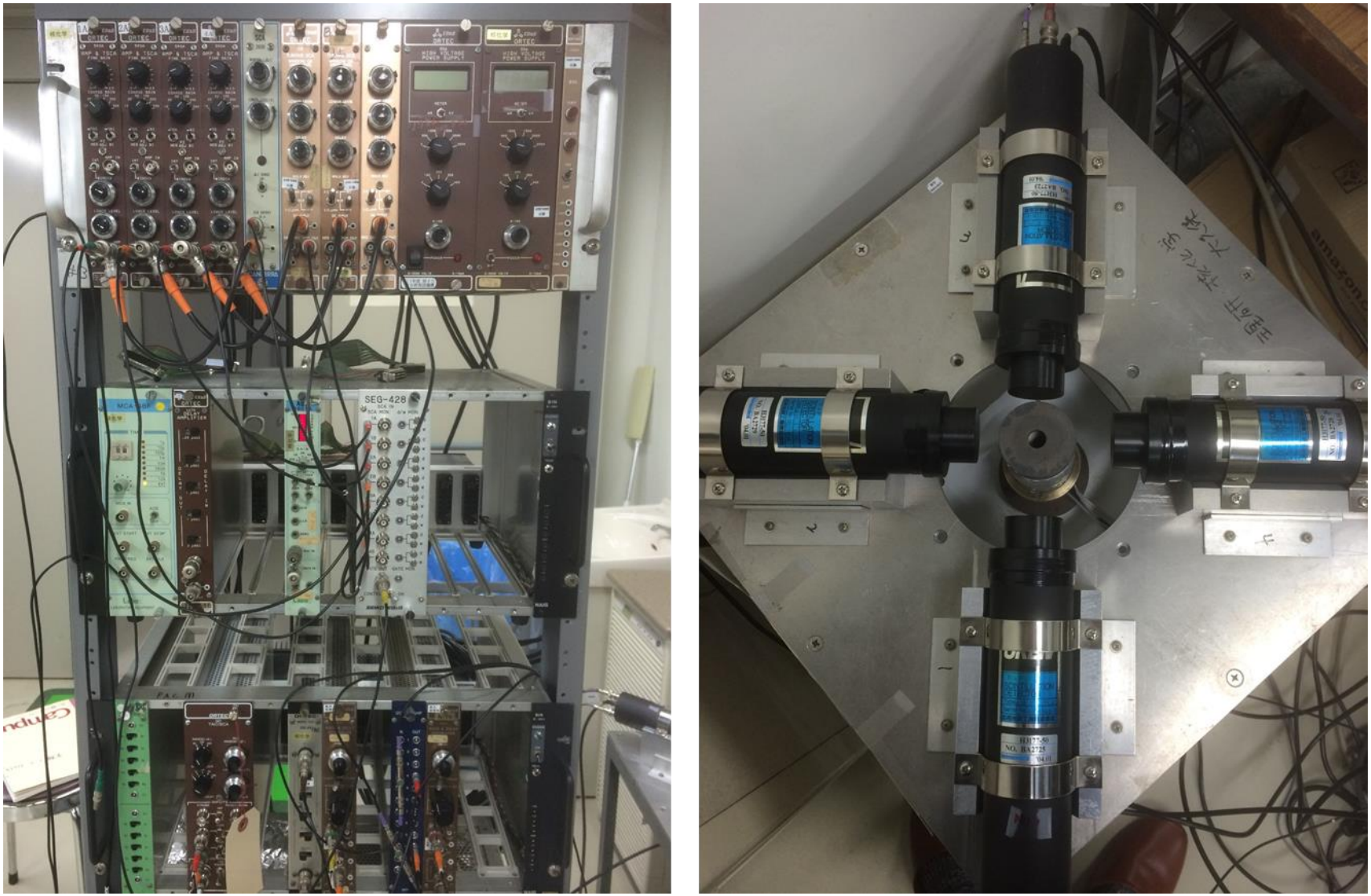

(a) A data taking circuitry for the present TDPAC measurements

(b) Four-detector system of $\pi/2$ and π directions

Fig. 6 Pictures of experimental setup of the present TDPAC measurements

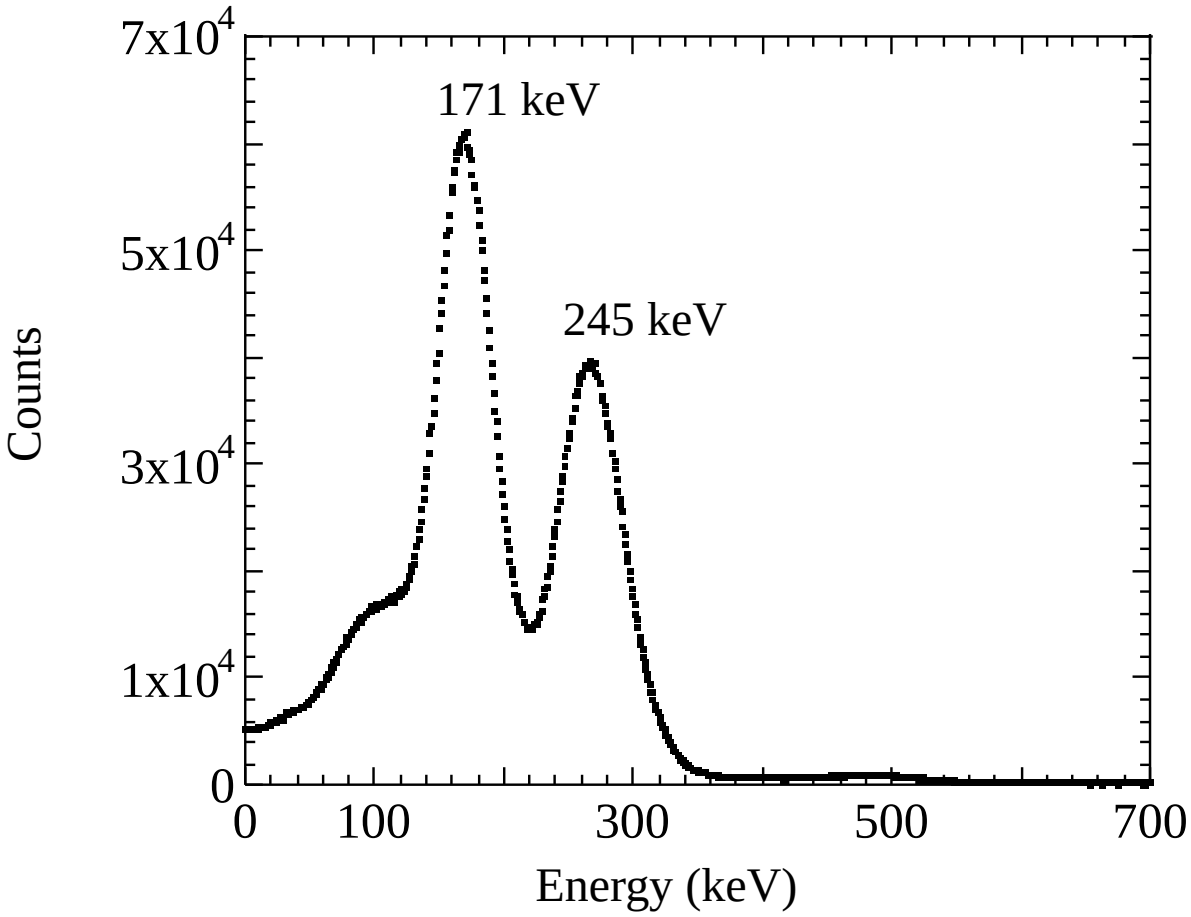

Fig. 7 Typical γ-ray energy spectrum of ^{111}In observed by the BaF_2 scintillators

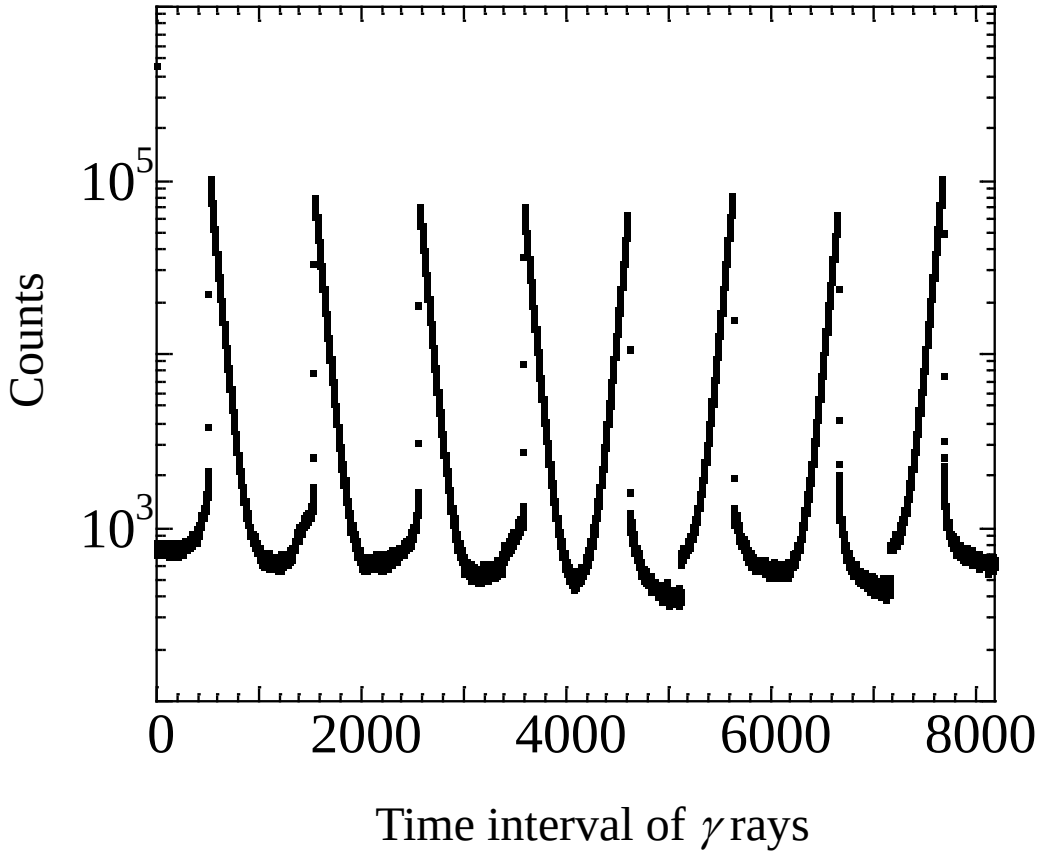

Fig. 8 Typical time-dependent delayed coincidence events at the time interval of the cascade γ-ray emissions

PART I

Stability of Al and In Impurities Doped in Zinc Oxide

Chapter 1 Al-Concentration Dependence of Local Structures in ZnO

1-1 Introduction

Future extrinsic-semiconductor devices such as of Al-doped ZnO are expected to be in use under various ambient conditions, and the states of being of impurity ions in the matrix changes depending on the condition. When exposed to heat, for example, their thermal diffusion could take place among lattice sites. In the process of the diffusion, impurity Al ions plausibly have chances to be adjacent to each other; the chance encounter may give rise to the formation of different stable structure(s) of their own (as suggested in Ref. [26]), which would lead to alteration of the bulk properties. The frequency of the chance encounter is thus considered to be an important factor that determines the bulk physical properties of the sample as well as the local structures of Al ions. It is therefore important to investigate the relation between the relevant frequency and the possible alteration of local structures for a wide application of the semiconductor.

Taking into account the fact that the frequency of the chance encounter directly depends on the concentration of Al ions, the concentration dependence of the TDPAC spectra for 10^{-6} to 10 at.% Al-doped ZnO were examined. In this chapter, the local environment of Al atoms doped in ZnO at various concentrations is discussed.

1-2 Experiment

Zinc oxide samples doped with various Al concentrations were separately synthesized by a solid-state reaction according to the following procedure, which is schematized in Fig. 9 for better understanding. Soichiometric amount of $Al(NO_3)_3 \cdot 9H_2O$ of a purity of 99.9% was dissolved in ethanol, and then ZnO powder (99.999%)

was added in the solution. The suspension was stirred while heated to evaporate the ethanol until dryness. The uniformly mixed powder was then pressed into disks and sintered on platinum plates in air at 1273 K for 3 h. Commercially available ^{111}In HCl solution was added in droplets onto the sintered disks. The initial concentration of ^{111}In ions doped in the sample was typically ~100 ppt. After the disks were dried up by heat, they again underwent heat treatment in air at 1373 K for 2 h. Following the doping of ^{111}In, the disks were separately ground into powder and sealed in quartz tubes. The TDPAC measurements were carried out at room temperature for the 171-245 keV cascade γ rays of the ^{111}In($\rightarrow^{111}$Cd) probe with the intermediate state of I = 5/2 having a half-life of 85.0 ns.

1-3 Results and Discussion

For easy understanding of the effect of the Al doping on the present perturbation pattern, the TDPAC spectrum of ^{111}In($\rightarrow^{111}$Cd) in undoped ZnO is firstly cited in Fig. 10 from previous studies[21]. Figure 11 shows the TDPAC spectra for the Al-doped ZnO at various concentrations. The spectrum for the undoped ZnO in Fig. 10 exhibits an oscillatory structure typical of the electric quadrupole interaction between the probe nucleus and the extranuclear field (hereafter denominated Component I). As for the Al-doped ZnO, although the oscillating pattern reproducible with a single component is not clearly discernible due to the damped structure reflecting a wide distribution of the field at the probe, the static perturbation pattern for the Al-doped ZnO in Fig. 11 (denominated Component II) is also ascribable to the electric quadrupole interaction because the sample consists of no magnetic materials; accordingly, the perturbation pattern distinct from that for Component I should be attributed to the change in the charge distribution around the

probe by the Al doping. The least squares fits were thus performed for the spectra in Fig. 11 with $G_{22}(t)$ expressed as

$$G_{22}(t)=G_{22}^{*}(t)\left[S_{2,0}+\sum_{n=1}^{3}S_{2,n}\exp(-\frac{1}{2}\delta^{2}\omega_{Q_n}^{2}t^{2})\cos(\omega_{Q_n}t)\right], \qquad (9)$$

where $G_{22}^{*}(t)$ represents the dynamic perturbation part for the spectral damping caused by the aftereffect characteristic of the EC decay of ^{111}In[27]. $G_{22}^{*}(t)$ is described as

$$G_{22}^{*}(t)=\frac{\lambda_g}{\lambda_g-\lambda_r}+\frac{\lambda_r}{\lambda_g-\lambda_r}\exp\left[-(\lambda_g-\lambda_r)t\right], \qquad (10)$$

where λ_g is defined as the reciprocal of the recovery time, τ_g, to the ground state of the probe atom, and λ_r stands for the Abragam and Pound relaxation constant[28]. In Eq. (9), $S_{2,n}$ are functions only of the asymmetry parameter $\eta=(V_{xx}-V_{yy})/V_{zz}$ $(0\le\eta\le1)$ for the principal axes of the electric field gradient (EFG) chosen as $|V_{xx}|\le|V_{yy}|\le|V_{zz}|$, and ω_{Q_n} are related to the electric quadrupole frequency, ω_Q, in such a way as $\omega_{Q_1}=6\omega_Q$, $\omega_{Q_2}=12\omega_Q$, and $\omega_{Q_3}=18\omega_Q$, for the asymmetry parameter $\eta=0$, for example. Gaussian distribution with its relative width δ is assumed for the quadrupole frequencies. The parameter values obtained by the least squares fits with Eq. (9) are listed in Table 2.

As already discussed in Ref. [21] for the spectrum of the undoped ZnO in Fig. 10, the EFG value at the ^{111}Cd nucleus corresponds to the ^{111}In ($\rightarrow^{111}$Cd) probe occupying the defect-free substitutional Zn site; the EFG value ($1.7(3)\times10^{21}$ V/m^2) obtained from the fit to the spectrum shows good agreement with theoretical values estimated for a Cd^{2+} ion residing at the Zn site (1.565×10^{21} and 1.68×10^{21} V/m^2) [29, 30]. As for the

TDPAC spectra in Fig. 11, the frequency component having a damping structure arises from the interaction between the ^{111}Cd($\rightarrow^{111}$In) probe and Al ions formed in the process of their thermal diffusion in air at 1373 K. The δ value of Component II is quite large as listed in Table 2. The widely distributed EFG may arise from the probes adsorbed to various grain boundaries of Al aggregations. (Detailed discussion on the Al local structure is described in Chapter 2) In spite of the large concentration gap, there is not a noticeable difference between the spectra in Fig. 11(a) and Fig. 11(f) in terms of the EFG values, which signifies that most of the probe ions of about 100 ppt can "find out" the Al ion(s) in ZnO matrix despite the low Al concentration of 10^{-3} at.%. As shown in Fig. 11(g), however, Component I in the 10^{-4} at.% Al-doped sample makes a slight appearance compensating for the loss of Component II. Furthermore, coexistence of Components I and II has become more visible in Figs. 11(h) and (i). This observation is depicted in Fig. 12 showing the fractions of Components I and II as functions of the Al concentration. The increase/decrease correlation is seen between their fractions. It is at this low concentrations of 10^{-6}~10^{-4} at.% that the probe ions gradually come to reside solely at the substitutional Zn site being independent of the field produced by the Al ions. Considering this phenomenon from the opposite point of view, it is remarkable that the ^{111}In($\rightarrow$ ^{111}Cd) probe can be associated with Al ion(s) at this extremely dilute concentration. This association is presumably attained by their chance encounter in the process of their thermal diffusion in solid ZnO; once they meet each other, the ^{111}In($\rightarrow$ ^{111}Cd) probe would be trapped in the field of Al ion(s), resulting in the formation of non-unique local structures as suggested by the wide distribution of the EFG. The present observations may thus suggest that there is a strong attractive force between the group 13 elements, In and Al, on this atmospheric condition.

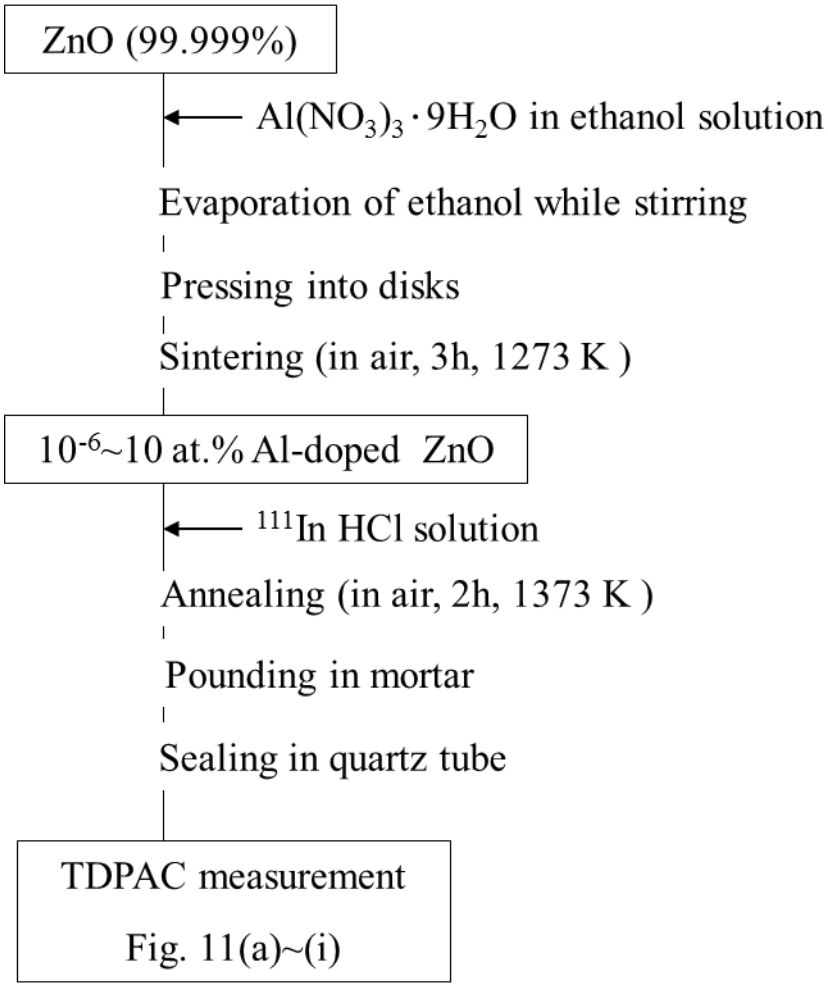

Fig. 9 Experimental procedure of sample preparation and TDPAC measurements for 10^{-6}~10 at.% Al-doped ZnO.

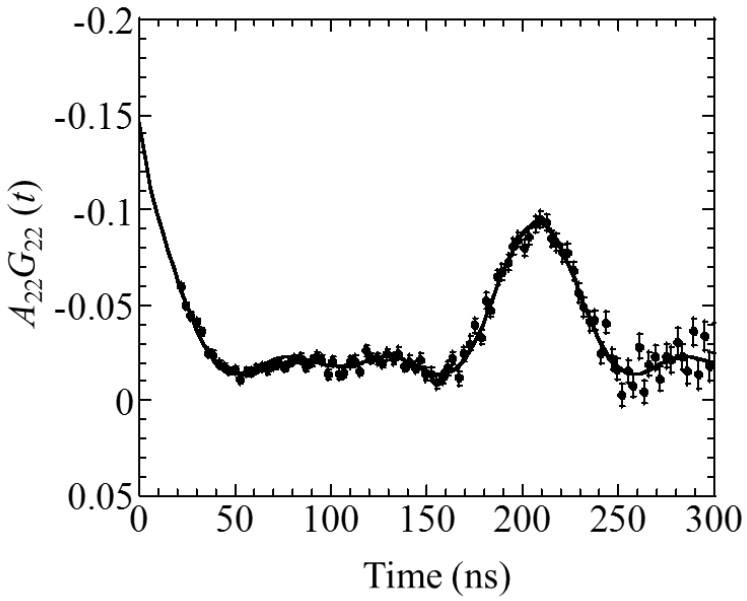

Fig. 10 TDPAC spectrum of ^{111}In(→^{111}Cd) in undoped ZnO measured at room temperature. (Cited from Reference [21])

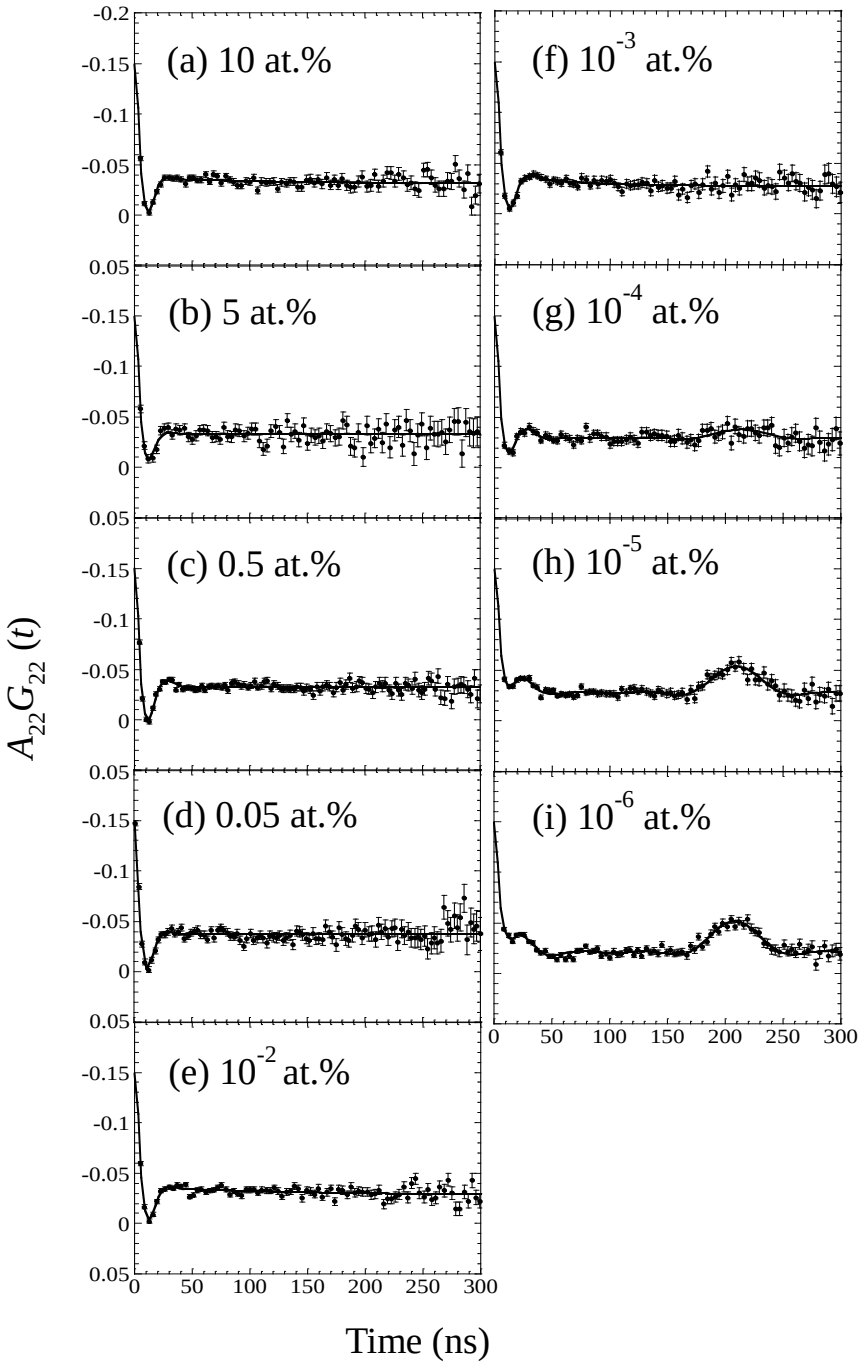

Fig. 11 TDPAC spectra of ^{111}In(→^{111}Cd) in 10^{-6}~10 at.% Al-doped ZnO measured at room temperature. Al concentration is indicated.

Table 2 Parameter values obtained by least-squares fits on the TDPAC spectra of $^{111}In(\rightarrow^{111}Cd)$ in undoped and in 10^{-6}~10 at.% Al-doped ZnO.

Corresponding spectrum	Al concentration (at.%)	Component	Site assignment	V_{zz} ($10^{21}V/m^2$)	δ (%)	Fraction (%)
Fig. 10	Starting sample[21]	I	substitutional Zn site	1.7(3)	0	87(1)
Fig. 11(a)	10	II	In-Al aggregation	8.2(13)	42(3)	99(2)
Fig. 11(b)	5	II	In-Al aggregation	8.0(13)	23(6)	88(2)
Fig. 11(c)	0.5	II	In-Al aggregation	8.6(14)	34(4)	97(3)
Fig. 11(d)	0.05	II	In-Al aggregation	8.6(14)	40(5)	98(4)
Fig. 11(e)	10^{-2}	II	In-Al aggregation	7.9(13)	43(3)	100(2)
Fig. 11(f)	10^{-3}	II	In-Al aggregation	7.8(13)	37(5)	95(3)
Fig. 11(g)	10^{-4}	I	substitutional Zn site	1.7(3)	0	9(3)
		II	In-Al aggregation	8.3(14)	29(8)	82(3)
Fig. 11(h)	10^{-5}	I	substitutional Zn site	1.7(3)	0	30(3)
		II	In-Al aggregation	8.6(14)	33(6)	63(2)
Fig. 11(i)	10^{-6}	I	substitutional Zn site	1.7(3)	0	35(2)
		II	In-Al aggregation	8.5(14)	24(6)	57(2)

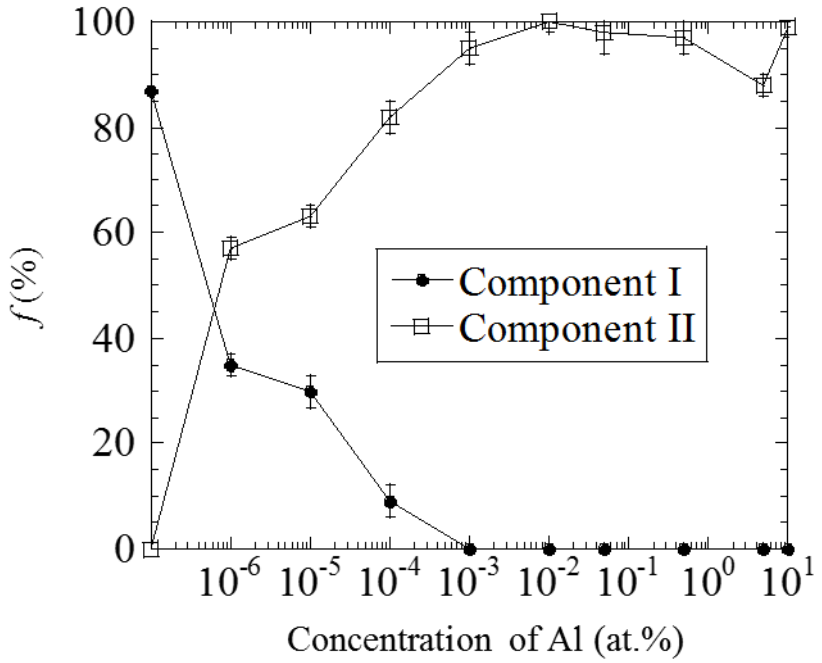

Fig. 12 Fractions of Component I (●) and Component II (□) as functions of Al concentration.

Chapter 2 Dispersion State and Strong Affinity of Al and In Impurities Doped in ZnO

2-1 Introduction

As described in Chapter 1, it is suggested that there is a strong attractive force between In and Al in ZnO. For the purpose of investigating how ^{111}In probes aggregate with Al ions in ZnO, additional TDPAC measurements for 0.05~10 at.% Al-doped ZnO were performed with the same ^{111}Cd probe formed in the disintegration of a different parent nucleus, ^{111m}Cd($\rightarrow ^{111}$Cd). As observed in previous TDPAC study[31], site occupation of the probe atom generally depends on the parent nucleus. Therefore, ^{111m}Cd($\rightarrow ^{111}$Cd) is expected to show different interaction with Al from these for the case of the ^{111}In($\rightarrow ^{111}$Cd) probe during their thermal diffusion process, which would provide detailed information on how Al ions reside in ZnO. In this chapter, dispersion state of Al ions in ZnO is discussed based on different interacting natures between Al and the probes (^{111}Cd) formed in the disintegration of different parents (^{111}In and ^{111m}Cd).

2-2 Experiment

The site occupied by the ^{111m}Cd($\rightarrow ^{111}$Cd) probe in ZnO lattice was initially investigated according to the following procedure, which is schematized in Fig. 13 for better understanding. About 3 mg of cadmium oxide (CdO) enriched with ^{110}Cd was irradiated with thermal neutrons in a pneumatic tube at Kyoto University Reactor, and radioactive ^{111m}Cd was generated by the ^{110}Cd(n, γ)^{111m}Cd reaction. The neutron-irradiated CdO powder was then added into stoichiometric amount of ZnO powder to synthesize 0.5 at.% Cd-doped ZnO. The powders were thoroughly mixed in a mortar. The mixture was then pressed into a disk, and sintered in air at 1373 K for 45 min. A

TDPAC measurement was carried out for the ^{111m}Cd($\rightarrow^{111}$Cd) probe on the 151–245 keV cascade γ rays with the intermediate state of $I = 5/2^+$ having a half-life of 85.0 ns.

After ascertaining the residence site of the ^{111m}Cd($\rightarrow^{111}$Cd) probe, which is described in Section 2-3, the interacting nature of Al and Cd ions was investigated in the following manner. 0.05~10 at.% Al-doped ZnO powder samples were prepared in the procedure described in Section 1-2. CdO powder including the ^{111m}Cd($\rightarrow^{111}$Cd) probe prepared in the same way as above was mixed with the Al-doped ZnO samples. The mixtures were subsequently pressed into disks and sintered in air at 1373 K for 45 min. TDPAC measurements were performed for the samples at room temperature.

2-3 Results and discussion

Figure 14 shows the TDPAC spectra of ^{111m}Cd($\rightarrow^{111}$Cd) in 0.5 at.% Cd-doped ZnO and in 0.5 at.% Cd- and Al-doped ZnO. It is to be noted that the 0.5 at.% nonradioactive Cd is inevitably incorporated in the sample because the nuclear isomer ^{111m}Cd cannot be chemically separated from the stable ^{110}Cd in the irradiated CdO. The oscillatory structures observed in the spectra in Fig. 14 are typical of the perturbation pattern reflecting an axially symmetric static electric quadrupole interaction for the nuclear spin $I = 5/2$. Assuming a asymmetric static EFG, a least-squares fit was carried out for the spectrum in Fig. 14 using the following time-differential perturbation factor:

$$G_{22}(t)=\frac{1}{5}\left[1+\frac{13}{7}\cos(6\omega_Q t)+\frac{10}{7}\cos(12\omega_Q t)+\frac{5}{7}\cos(18\omega_Q t)\right]. \qquad (11)$$

The parameter values obtained by the least squares fits are listed in Table 3. For the TDPAC spectrum in Fig. 14(a), the magnitude of EFG at the probe was estimated to be

1.8(3)$\times 10^{21}$ Vm^{-2}. This observation demonstrates that the ^{111}Cd probe doped in 0.5 at.% Cd-doped ZnO resides at the substitutional Zn site. Regardless of Al concentration, the spectral patterns for all the Cd- and Al-doped ZnO samples are analogous to the one for 0.5 at.% Cd-doped ZnO, and the magnitudes of the EFGs agree well with each other. That is, even under the presence of a large amount of Al ions in the system, the ^{111m}Cd($\rightarrow$ ^{111}Cd) probe is not affected by the local field produced by the Al ions.

Considering the previous work of Ref. 31, this observation provides another interpretation about the Al local structure. For comparison, the TDPAC spectra for ^{111m}Cd($\rightarrow^{111}$Cd) in 0.5 at.% Cd- and 2~10 at.% In-doped ZnO are cited in Fig. 15 from our previous studies[31]. This observation demonstrates that the ^{111m}Cd($\rightarrow^{111}$Cd) probe doped in Cd- and In-doped ZnO also resides at the substitutional Zn site regardless of the presence of In impurities in the system. As is distinct from Fig. 14(b)~(e) (Cd- and Al-doped ZnO), the distribution of the quadrupole frequencies becomes greater with increasing concentration of the doped In. The distribution can be an index of diversity of the environment surrounding the ^{111m}Cd($\rightarrow^{111}$Cd) probe. In view of this, the above observation provides a finding that In ions are widely dispersed. Little spectral change seen for the Cd- and Al-doped ZnO in Fig. 14 suggests that Al ions are not scattered one by one but are likely to form island-like aggregation of their own. (Schematic illustration of state of being of ^{111}In from Al ions is shown in Fig. 16.) It was also confirmed from X-ray diffraction patterns of Al-doped ZnO in Figs. 17(a)~(b) that $ZnAl_2O_4$ is deposited as an independent phase in 5 and 10 at. % Al-doped ZnO. Taking it into consideration that the present sample is powder, the widely distributed EFG may originate from the probes adsorbed to various grain boundaries of such aggregations. From the TDPAC measurements for 10^{-6}~10 at.% Al-doped ZnO showing similar local

structures at the ^{111}In($\rightarrow^{111}$Cd) regardless of the large difference of Al concentrations, it can also be said that even ppm-level dilute Al impurities locally associate with each other to form such minute $ZnAl_2O_4$ grains that are undetectable by the present XRD detection precision.

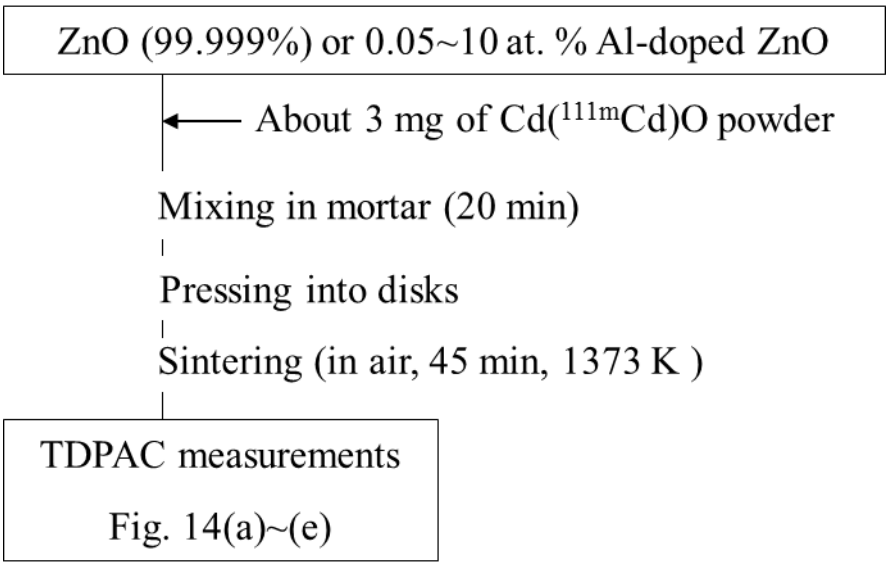

Fig. 13 Experimental procedure of sample preparation and TDPAC measurements for 0.5 at.% Cd- and 0.05~10 at.% Al-doped ZnO.

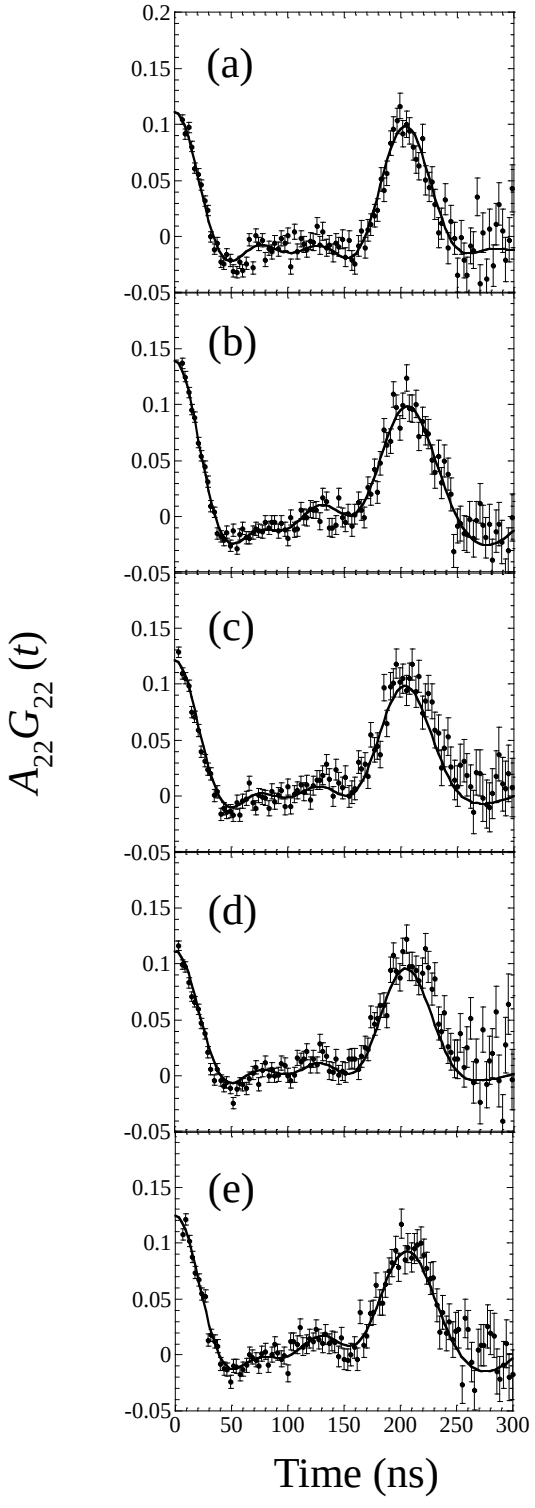

Fig. 14 TDPAC spectra of ^{111m}Cd($\rightarrow^{111}$Cd) (a) in 0.5 at.% Cd-doped ZnO, (b) in 0.5 at.% Cd- and 0.05 at.% Al-doped ZnO, (c) in 0.5 at.% Cd- and 2 at.% Al-doped ZnO, (d) in 0.5 at.% Cd- and 5 at.% Al-doped ZnO, and (e) in 0.5 at.% Cd- and 10 at.% Al-doped ZnO. TDPAC measurements were performed at room temperature.

Table 3 Parameter values obtained by least-squares fits on the TDPAC spectra of ^{111m}Cd($\rightarrow^{111}$Cd) in 0.5 at.% Cd-doped ZnO and in 0.5 at.% Cd- and 0.05 to 10 at.% Al-doped ZnO.

Corresponding spectrum in Fig. 14	Al concentration (at.%)	Site assignment	V_{zz} (10^{21}V/m^2)	δ (%)	Fraction (%)
(a)	0	substitutional Zn site	1.8(3)	5(1)	110(1)
(b)	0.05	substitutional Zn site	1.7(3)	8(1)	107(1)
(c)	2	substitutional Zn site	1.7(3)	6(1)	99(1)
(d)	5	substitutional Zn site	1.7(3)	5(1)	97(1)
(e)	10	substitutional Zn site	1.7(3)	7(1)	101(1)

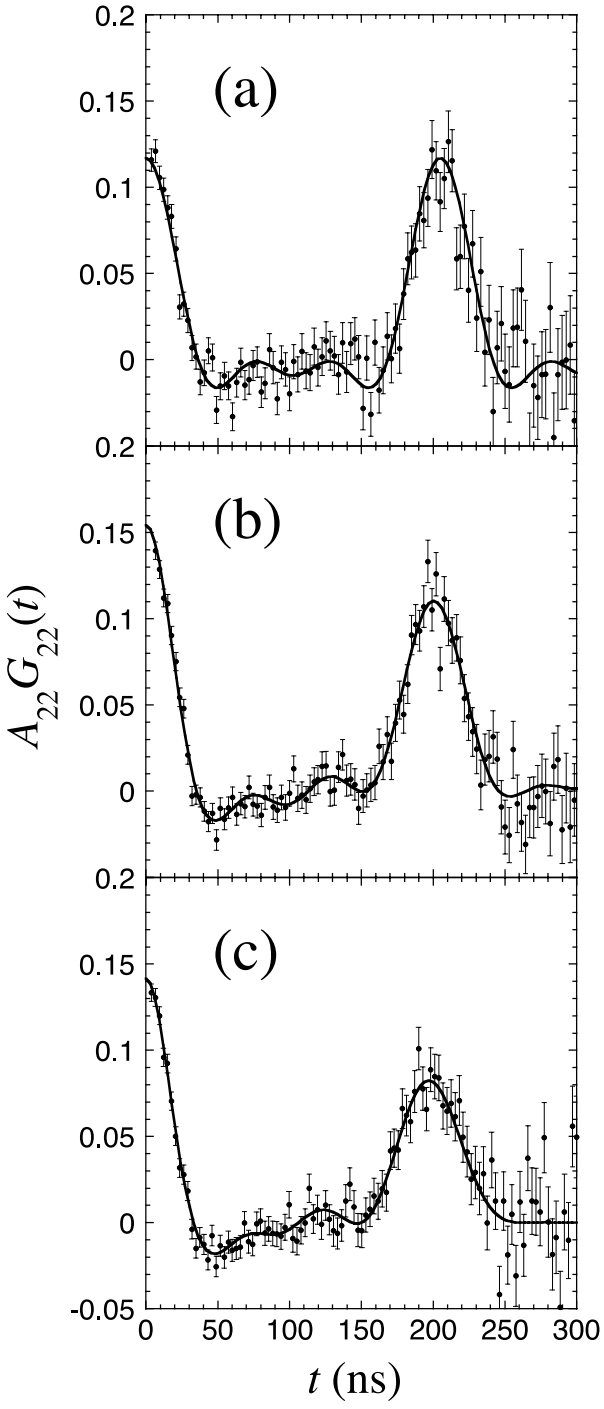

Fig. 15 TDPAC spectra of ^{111m}Cd($\rightarrow^{111}$Cd) (a) in 0.5 at.% Cd-doped ZnO, (b) in 0.5 at.% Cd- and 0.5 at.% In-doped ZnO, (c) in 0.5 at.% Cd- and 2 at.% In-doped ZnO. TDPAC measurements were performed at room temperature. (Cited from reference [31])

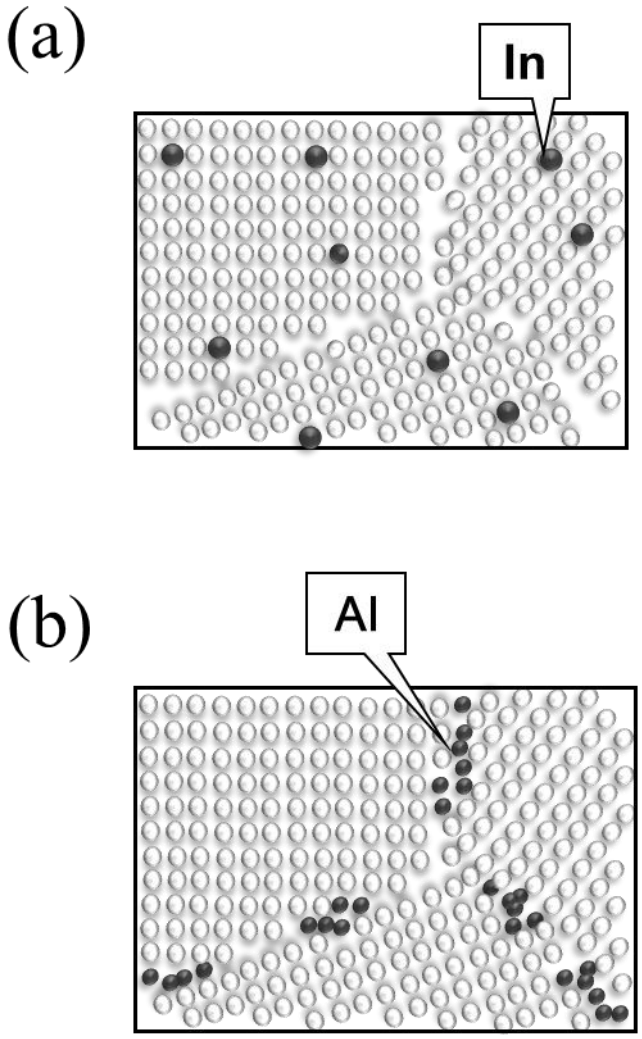

Fig. 16 Schematic illustration of the state of being of (a) In and (b) Al impurities distributed in ZnO.

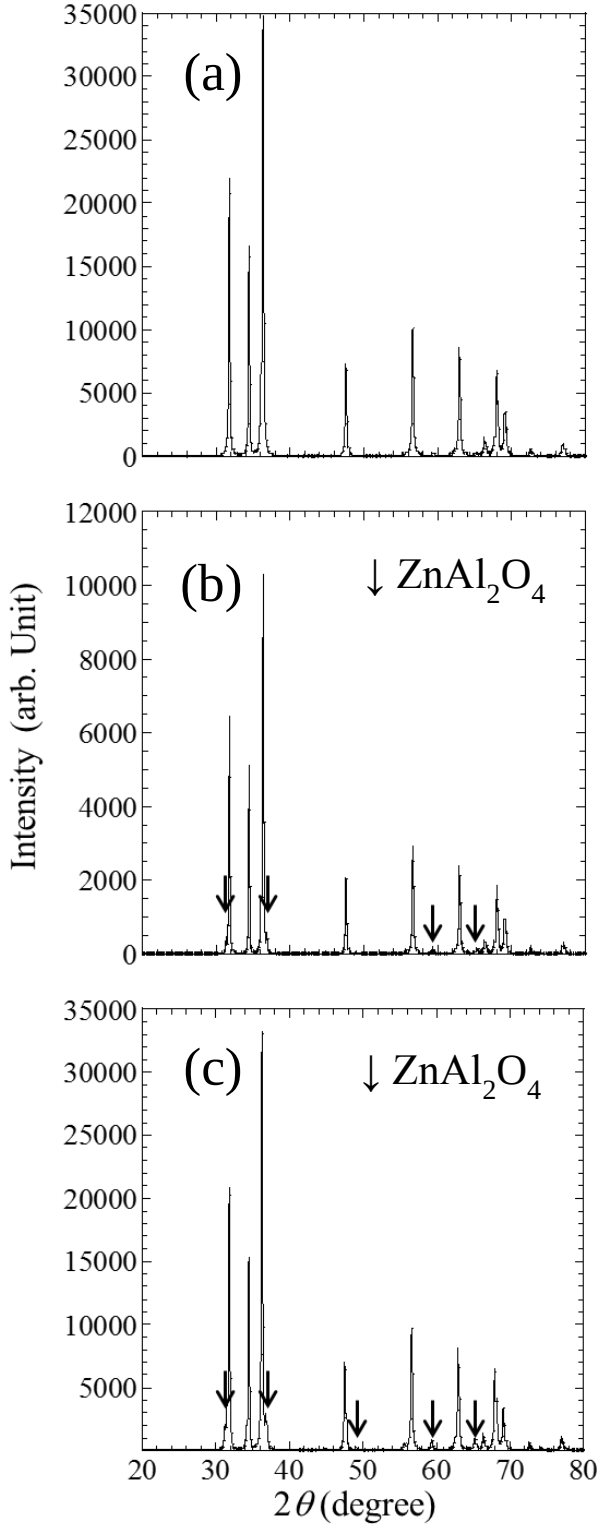

Fig. 17　Powder X-ray diffraction patterns (a) of 2 at.% Al-doped ZnO, (b) of 5 at.% Al-doped ZnO, and (c) of 10 at.% Al-doped ZnO

Chapter 3 Temperature Dependence of Local Structures Formed by Al Ions

3-1 Introduction

In Section 1-3, the effect of Al concentration on the local structure was discussed. It was suggested from the observation that the ^{111}In($\rightarrow^{111}$Cd) probe is associated with Al ion(s) of extremely dilute concentration (0.01 ppm). This association is attained by their chance encounter in the process of their thermal diffusion in solid ZnO; once they meet each other, the ^{111}In($\rightarrow^{111}$Cd) probe would be trapped in the field of Al ion(s).

Apart from Al concentration, the chance encounter of impurities in solid ZnO is also controlled by diffusion temperature. For example, if heat treatment is conducted at high temperature, the jump frequency of impurity ions is increased due to enough activation energy to go over the potential, resulting in the enhancement of the chance encounter of Al ions. In the same way as the study of Al-concentration dependence, therefore, it is also important to investigate temperature dependence of local structures formed by Al ions. In this chapter, temperature dependence of thermal behavior of Al ions is discussed based on TDPAC spectra of the ^{111}In($\rightarrow^{111}$Cd) in 0.5 at.% Al-doped ZnO prepared by annealing at different temperatures.

3-2 Experiment

Because the purpose of the present experiment is to examine the diffusion process of Al impurities, ^{111}In probe nuclei as the “eyes” to watch the thermal behavior of the Al impurities should be settled first at a defined site; Al impurities were then introduced in the ^{111}In-ZnO sample at various temperatures as explained in the next paragraph. (Because the ionic radius of In^{3+} (63 pm) is much larger than that of Al^{3+} (39 pm) when coordinated by 4 ions[32], it is considered that higher thermal energy is needed

for diffusion of In^{3+} among ZnO lattice. Preceding introduction of Al ions, conducted at lower temperatures, is therefore inappropriate for the present purpose because the following introduction of the ^{111}In probe at higher temperature would alter the local structures formed through the temperature-dependent diffusion process of Al ions.) In the present experiment, sufficient amount of Al (0.5 at.%) was introduced to ZnO for the purpose of securely observing the association process of Al and In ions.

The sample preparation was performed by the following procedure, which is schematized in Fig. 18. ZnO powder of a purity of 99.999% was pressed into disks and sintered on platinum plates in air at 1273 K for 3 h. Commercially available ^{111}In HCl solution was added in droplets onto the sintered disks. The initial concentration of ^{111}In ions doped in the sample is typically ~100 ppt. After the disks were dried up by heat, they again underwent heat treatment in air at 1373 K for 2 h. After the doping of ^{111}In impurity, stoichiometric amount of $Al(NO_3)_3 \cdot 9H_2O$ of a purity of 99.9% dissolved in distilled water was added in droplets onto the disks of undoped ZnO for the synthesis of 0.5 at.% Al-doped ZnO. After the disks were dried up by heat, they were respectively ground into powder homogeneously. Then powder samples were separately pressed into disks again and each of them underwent heat treatment in air at 873, 973, and 1373 K for 20 h, respectively. The TDPAC measurements were carried out at room temperature for the 171-245 keV cascade γ rays of ^{111}In($\rightarrow^{111}$Cd) probe with the intermediate state of I = 5/2 having a half-life of 85.0 ns.

3-3 Results and Discussion

For the examination of the diffusion process of Al impurities doped in ZnO, the ^{111}In probe nuclei as the “eyes” to watch the thermal behavior of the Al impurities should

be settled first at a defined site. The probe was thus firstly introduced into the substitutional Zn site, and subsequently, Al ions were introduced into the sample to obtain clear information on locally occurring structural alteration. Figure 19 shows the TDPAC spectrum of ^{111}In($\rightarrow ^{111}$Cd) obtained for the undoped ZnO. The parameter values obtained by the least squares fits with Eq. (9) are listed in Table 4. From the fit, it was confirmed that the TDPAC spectrum in Fig. 19 consists of a single component of a unique quadrupole frequency. It has already been known from our previous TDPAC study for undoped ZnO[21] that the ^{111}In($\rightarrow ^{111}$Cd) probe occupies the substitutional Zn sites by sufficient annealing at 1373 K for 2 h.

After the introduction of the ^{111}In($\rightarrow ^{111}$Cd) probe into the substitutional Zn site, the annealing temperature dependence of the local structure of Al and In was investigated. Figure 20 shows the TDPAC spectra for 0.5 at.% Al-doped ZnO prepared by heat treatment in air (a) at 873, (b) at 973, and (c) at 1373 K, respectively. The parameter values obtained by least squares fits with Eq. (9) are listed in Table 4. The spectrum of Fig. 20(a) is principally made up of only Component I, suggesting that the ^{111}In($\rightarrow ^{111}$Cd) probe does not feel the field of Al remaining in defect-free substitutional Zn site after heat treatment at 873 K in air. For the spectrum of Fig. 20(b), however, the spectral peak arising from Component I is damped, and another structure (Component II) appears at around 20 ns by the heat treatment process at 973 K. Because this structure was emerged by Al doping, the relevant component reflects the interaction between the ^{111}In($\rightarrow ^{111}$Cd) probe and Al ion(s) in ZnO. Furthermore, for the TDPAC spectrum of Fig. 20(c), Component II has become dominant, having the fraction of 78 (1)%, which means that most of the probe ions reside in the vicinity of Al ions as a result of the heat treatment process at 1373 K in air. From all the observations above, it is suggested that local

association of Al and In ions does not occur at temperature as low as 873 K, but thermal energy given at 973 K can cause the impurity ions to form local aggregation.

Then, how do the ^{111}In($\rightarrow^{111}$Cd) probe and Al ions form aggregations by their thermal diffusion at 973 K? There are two possible candidates for the aggregation process: (1) Al ions thermally diffuse in ZnO matrix and nucleation takes place at the ^{111}In($\rightarrow^{111}$Cd) probes "fixed" at the substitutional Zn sites, or (2) ^{111}In ions "hop around" from the substitutional Zn site to site to find Al ions already assembled by their diffusion. The former candidate (1) is derived from the picture that ^{111}In ions are stabilized in the potential at the substitutional Zn site at which Al ions gather in the process of their thermal diffusion. This interpretation of the aggregation process suggests that only Al ions can move around at 973 K. For the latter candidate (2), on the other hand, a site-to-site movement of ^{111}In ions is assumed. As shown in Ref. [21], a TDPAC spectrum of the probe substituting for Zn shows, reflecting static perturbation, explicit oscillatory structure even measured at 1000 K, which appears contradictory to the above assumption (2). However, this observation does not necessarily mean that ^{111}In ions are fixed at the substitutional position without jumping around; even if the probe is in motion among Zn sites, an oscillatory structure could appear in the spectrum when the time scale of the jump frequency is much larger than the time interval of the cascade γ-ray emissions from the probe, which may be typically in the order of millisecond or more in the present case. Accepting this regime, the 20-hour heat treatment is sufficient for ^{111}In to hop around among Zn sites to be trapped by the relevant aggregations of Al ions. In either case, (1) or (2), once the probe is trapped in the field of Al ions during the thermal diffusion process, the bound state is very stable and does not dissociate in air. The above observation suggests that local association of Al and In ions formed in ZnO is stable against the heat

treatment and the aggregation process is irreversible in air.

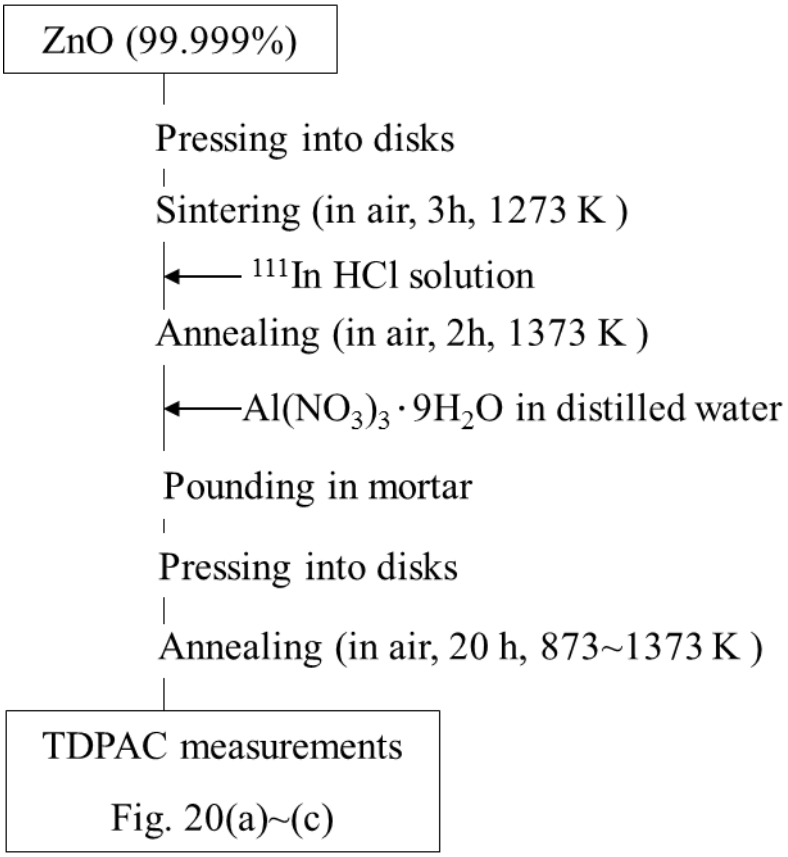

Fig. 18 Experimental procedure of sample preparation and TDPAC measurements for 0.5 at.% Al-doped ZnO

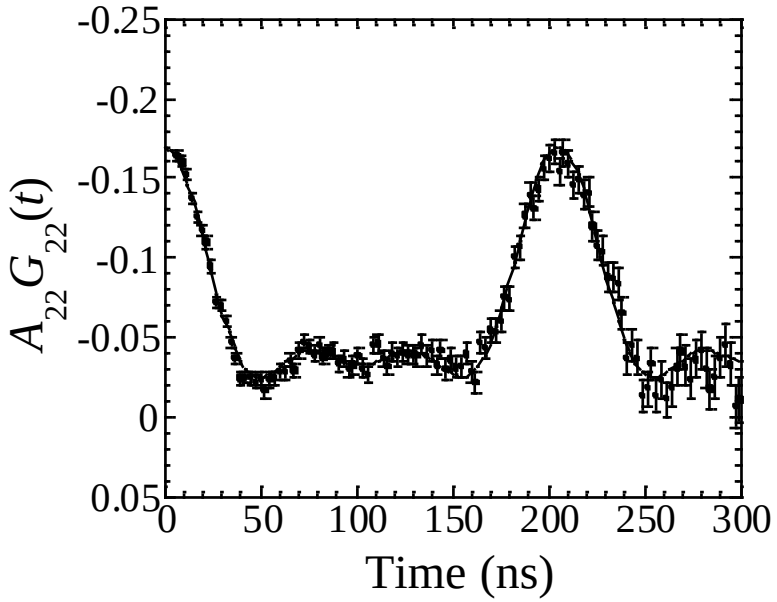

Fig. 19 TDPAC spectrum of ^{111}In($\rightarrow$ ^{111}Cd) in undoped ZnO. TDPAC measurement was performed at room temperature.

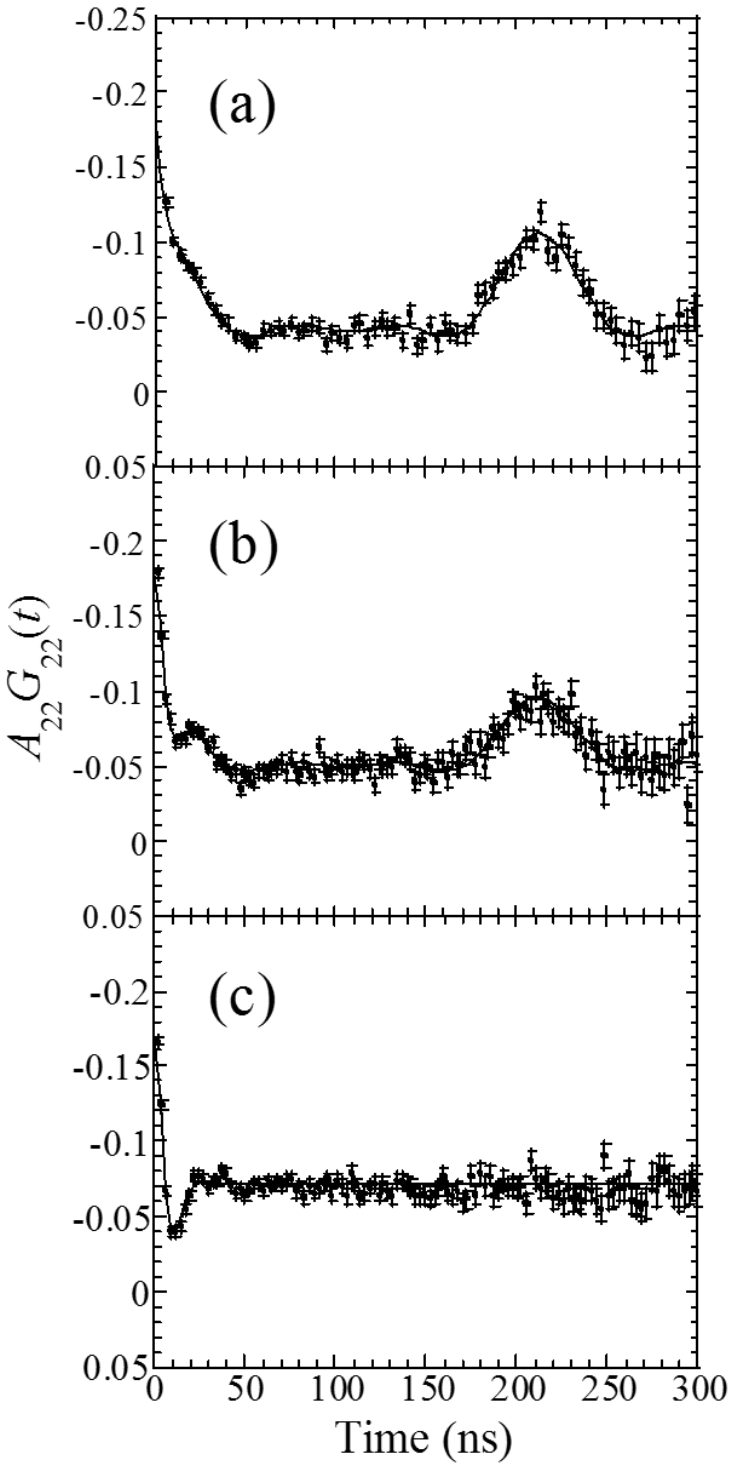

Fig. 20 TDPAC spectra of ^{111}In($\rightarrow^{111}$Cd) in 0.5 at.% Al-doped ZnO annealed in air (a) at 873 K, (b) at 973 K, and (c) at 1373 K. TDPAC measurements were performed at room temperature.

Table 4 Parameter values obtained by least-squares fits on the TDPAC spectra of ^{111}In($\rightarrow^{111}$Cd) in undoped ZnO and in 0.5 at.% Al-doped ZnO.

Annealing temperature (K)	Component	Site assignment	V_{zz} (10^{21}V/m^2)	δ (%)	Fraction (%)
Starting sample	I	substitutional Zn site	1.7(3)	0	78(1)
873	I	substitutional Zn site	1.7(3)	0	76(1)
973	I	substitutional Zn site	1.7(3)	0	25(2)
	II	In-Al aggregation	8.6(14)	50(5)	63(2)
1373	II	In-Al aggregation	9.2(15)	40(2)	78(1)

Chapter 4 Atmosphere Dependence of Local Structures Formed by Al Ions

4-1 Introduction

It is known that local structures of metal oxide depend on atmosphere condition during heat-treatment because in oxide compounds, in general, oxygen vacancies are likely to be formed during annealing process at a lower partial pressure of atmospheric oxygen[33-35], and they may affect local structures of Al-doped ZnO as well. For detailed understanding of thermal behavior of doped Al impurities, therefore, it is essential to clarify their thermal stability at a lower partial pressure of atmospheric oxygen. Hence in this chapter, TDPAC measurements were performed for ^{111}In($\rightarrow^{111}$Cd) in Al-doped ZnO heat-treated in vacuum.

4-2 Experiment

A TDPAC spectrum of the ^{111}In($\rightarrow^{111}$Cd) probe in 10 ppm Al-doped ZnO heat-treated in vacuum was initially obtained according to the following procedure, which is schematized in Fig. 21. 10 ppm Al-doped ZnO powder were prepared in the same way as the procedure described in Section 1-2. Commercially available ^{111}In HCl solution was added in droplets onto the sintered disks. The initial concentration of ^{111}In ions doped in the sample was typically ~100 ppt. After the disks were dried up by heat, they underwent heat treatment in air at 1373 K for 2 h. Following the doping of ^{111}In, the disks were ground into powder and sealed in quartz tubes in vacuum. TDPAC measurement with ^{111}In($\rightarrow^{111}$Cd) in 10 ppm Al-doped ZnO were performed (a) at room temperature in vacuum, (b) at 1000 K in vacuum, (c) at room temperature in vacuum (to see the reproducibility), and (d) at 1000 K in air. The measurements were carried out for a single sample in series as stated.

Because the results obtained from the above experiment, which are described in the next section, created a need to examine the impurity behaviors during heat-treatment in argon gas, additional TDPAC measurements were performed. The detailed experimental procedure is described along with the purpose in Section 4-3.

4-3 Results and Discussion

Figure 22 shows the TDPAC spectra of ^{111}In($\rightarrow^{111}$Cd) in 10 ppm Al-doped ZnO measured (a) at room temperature in vacuum, (b) at 1000 K in vacuum, (c) at room temperature in vacuum, and (d) at 1000 K in air. The spectra were fitted with Eq. (9). The spectrum patterns of Fig. 22(a) reproduce that shown in Fig. 11(f), suggesting that the ^{111}In($\rightarrow^{111}$Cd) probe is locally associated with Al ions to form Component II. As shown in Fig. 22(b), however, an oscillatory pattern of undoped ZnO (Component I) appears compensating for the fractional reduction of the Component II. This signifies that the probe ions gradually come to reside solely at the substitutional Zn site at 1000 K in vacuum being independent of the field produced by Al ions. Furthermore it is suggested from the spectrum in Fig. 22(c) that the Component I remains after exposure to the air. As seen in the spectrum of Fig. 22(d) measured at 1000 K in air, however, Component I vanished and only Component II was observed again, which suggests that most of the probe ions are attracted again to Al ions at this condition. These observations clearly exhibit atmosphere dependence of the thermal stability of the locally-associated Al and In impurities. It is thus reasonable to propose the following scenario based on the observed phenomena: Al and In are strongly bound to each other in ZnO during heat treatment “in air”, whereas the ^{111}In probes are dissociated from the bound state in high-temperature vacuum to migrate into defect-free substitutional Zn sites.

Then, what is the cause of the dissociation of the ^{111}In probe? So as to corroborate the interpretation that this reaction is induced by a lower partial pressure of atmospheric oxygen, an additional TDPAC measurement was performed for the same sample annealed under argon gas flow.

For the sample preparation, 100-ppm Al-doped ZnO disks doped with the ^{111}In probe were prepared in air by the same procedure described in Section 1-2. The disk was ground into powder and annealed under argon gas flow at 1373 K for 24 h. A TDPAC measurement was performed at room temperature. Figure 23 is the TDPAC spectrum of ^{111}In($\rightarrow^{111}$Cd) for 100 ppm Al-doped ZnO annealed in Ar gas flow, and the spectrum was fitted with Eq. (9). Because Component I is partly (f = 32(2)%) observed, the dissociation of Al and ^{111}In is considered to have proceeded in the same way as the case for the sample heat-treated in vacuum. Therefore, this dissociation process is closely related to the presence of O_2 gas.

What is the mechanism of the dissociation of the ^{111}In probe? The dissociation process suggests that the local association of Al and ^{111}In becomes unstable in high-temperature anaerobic atmosphere. As described above, in general, oxygen vacancies are likely to be formed in oxide compounds during annealing process at a lower partial pressure of atmospheric oxygen[36]. In addition, the formation of oxygen vacancies proceeds at grain boundaries compared with those in the bulk[37]. For the present Al-doped ZnO as well, oxygen vacancies would be formed at grain boundaries in the local structures of ^{111}In–Al aggregations at grain boundaries (denominated $^{111}\mathrm{In}_{\mathrm{agg}}^{\mathrm{GB}}$–$\mathrm{Al}_{\mathrm{agg}}^{\mathrm{GB}}$). This discussion is supported by the experiments observation (See APPENDIX 3 and APPENDIX 4 for detail.) This process could cause the local formation of excess cations due to the loss of negatively charged oxygen ion(s), and ^{111}In ions are consequently

expelled to migrate into more stable substitutional Zn sites (denominated $^{111}In_{sub}$) to keep the local charge balance. (Schematic illustration of the dissociation process of ^{111}In is shown in Fig. 24.) As for Al impurities, however, they may be involved in local aggregations of $ZnAl_2O_4$, which would be far more stable toward the heat treatment in vacuum. To summarize the discussion, ^{111}In ions adsorbed at the grain boundaries of Al aggregations migrate into the ZnO bulk to occupy substitutional Zn sites by heat treatment in vacuum, while Al ions remain in the aggregations as shown by the following reaction equation:

$$^{111}In^{GB}_{agg} - Al^{GB}_{agg} \xrightarrow{\text{Annealing in vacuum}} {}^{111}In_{sub} + Al^{GB}_{agg}.$$

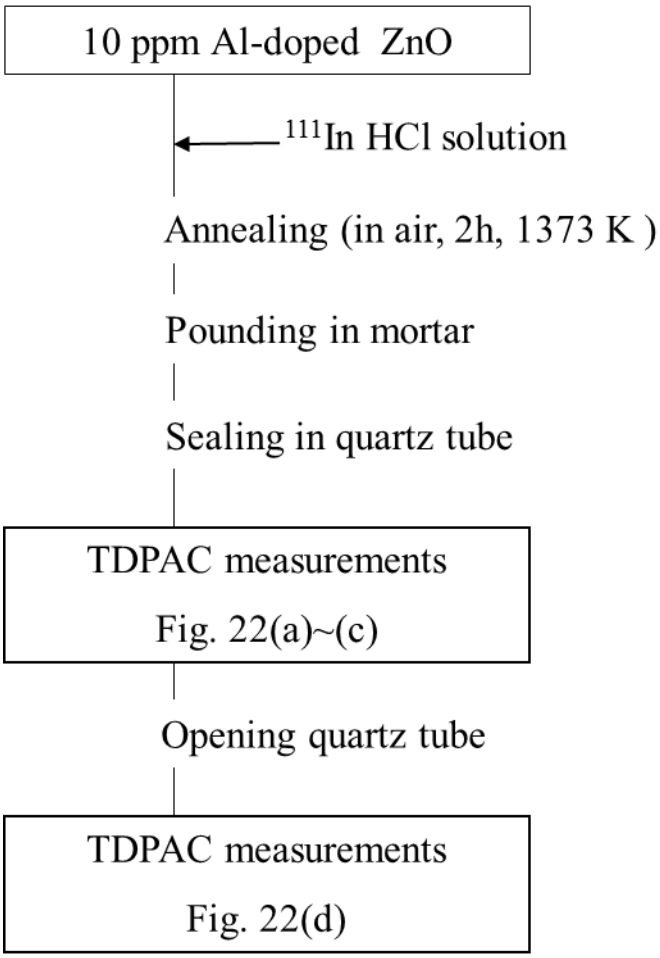

Fig. 21 Experimental procedure of sample preparation and TDPAC measurements for 10 ppm Al-doped ZnO

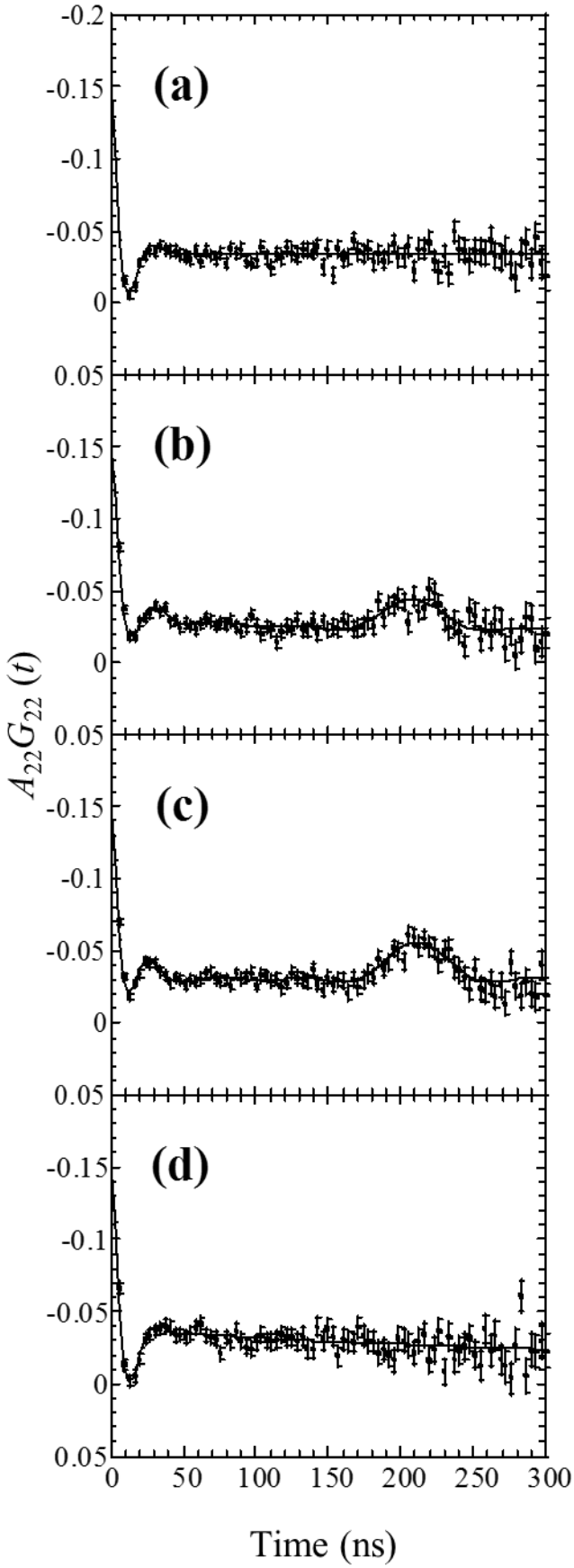

Fig. 22 TDPAC spetcta of ^{111}In(→^{111}Cd) in 10 ppm Al-doped ZnO observed (a) in vacuum at R.T., (b) in vacuum at 1000 K, (c) in air at R.T. and (d) in air at 1000 K. TDPAC spectra were measured in order of (a), (b), (c), (d).

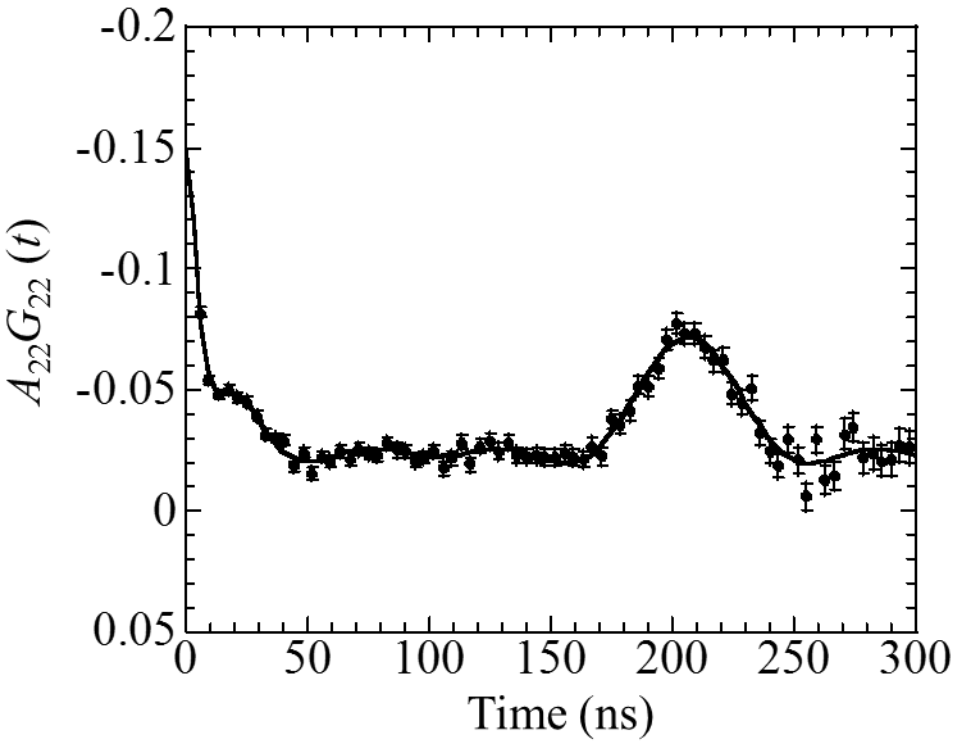

Fig. 23 TDPAC spetctum of ^{111}In($\rightarrow^{111}$Cd) in 100 ppm Al-doped ZnO annealed in argon gas flow. The TDPAC measurement was performed at room temperature.

(a) Association between ^{111}In and $ZnAl_2O_4$

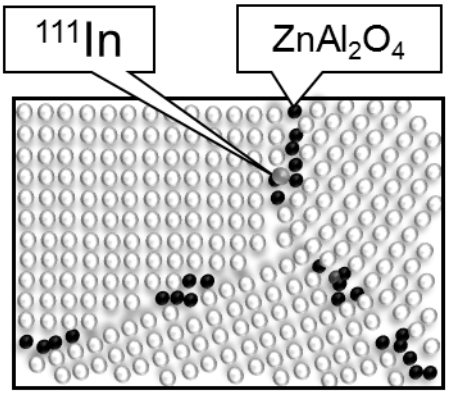

(b) Formation of oxygen vacancies

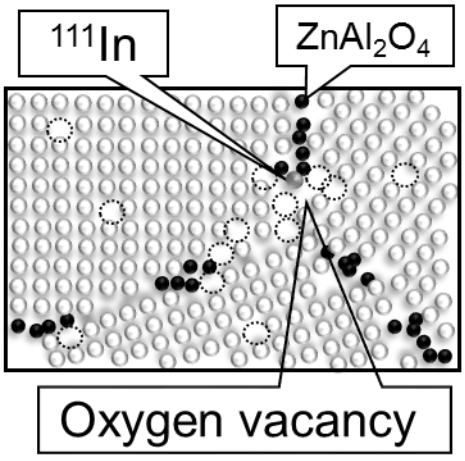

(c) Migration of ^{111}In ions

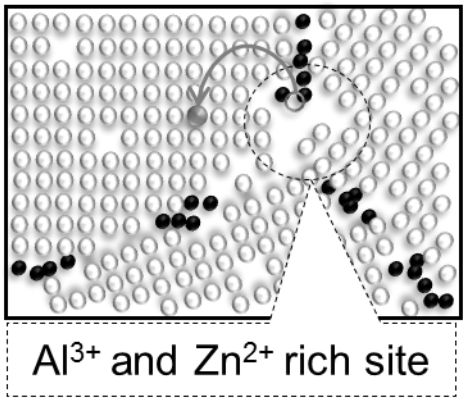

Fig. 24 Schematic illustration of the dissociation of ^{111}In process.

Chapter 5 Summary of PART I

In this study, TDPAC measurements with the ^{111}In($\rightarrow ^{111}$Cd) probe were performed for Al-doped ZnO heat-treated under various conditions to examine the following dependences of the formation of local structures of Al ions: Al concentration, temperature, and atmosphere. Contrasting interactions between Al and ^{111}In impurities were observed depending on the concentration of atmospheric oxygen to which the samples are exposed; (1) *in air*, Al impurities locally associate with each other to form minute $ZnAl_2O_4$ grains even at extremely dilute concentration of 0.01 ppm, and the ^{111}In($\rightarrow ^{111}$Cd) probe ions of about 100 ppt are trapped in the field of Al ion(s), but (2) *in vacuum*, the bound state of ^{111}In and Al formed in air dissociates by heat treatment at 1000 K, resulting in substitution of ^{111}In ions at defect-free tetrahedral Zn sites. Detailed investigation of the thermal behavior of the impurities has revealed that the dissociation reaction is triggered by the formation of oxygen vacancies in the vicinity of the locally-associated In-Al structure.

PART II

Formation Process of Oxygen Vacancy in Zinc Oxide

Chapter 1 Introduction

In PART I, thermal behavior of Al and In ions co-doped in ZnO was investigated by means of the TDPAC method with the ^{111}Cd probe. It was reported in Chapter 4 of PART I that in the process of thermal diffusion at 1373 K in air, In and Al impurities are locally associated with each other to form undefined aggregations, and this bound state of the aggregations is so stable "in air" that the ^{111}Cd($\leftarrow^{111}$In) probe once trapped in the potential produced by Al ions does not dissociate from the aggregation. In high-temperature vacuum, however, ^{111}In can be detrapped from the Al aggregations, resulting in substitution at defect-free Zn sites. Furthermore, in consideration of highly probable formation of oxygen vacancies in vacuum, it was proposed that the concentration of atmospheric oxygen controls the sites of the dilute impurities of ZnO. In general, it is known that oxygen vacancies affect the electric and optical properties in ZnO. Relating to this phenomenon, first-principles calculations have been conducted to obtain the formation energy of oxygen vacancies. (For example, Ref. [38]) To my knowledge, however, the experimental value of the formation energy of oxygen vacancies has not been reported so far.

For more quantitative information on the formation process of oxygen vacancies, in the present work, a unique method is presented for the estimation of the experimental activation energy of the oxygen-vacancy formation; TDPAC measurements were performed for the 100-ppm Al-doped ZnO prepared by isothermal and isochronal annealings in vacuum, and the observed results are quantitatively discussed based on the rate constant and the activation energy for the dissociation of the bound state of Al-In impurities.

Chapter 2 Experiments

2-1 Isothermal Annealing

The annealing-time dependence of the locally-associated In-Al structure is initially examined according to the following procedure, which is schematized in Fig. 25 for better understanding. For the synthesis of 100 ppm Al-doped ZnO, stoichiometric amount of $Al(NO_3)_3 \cdot 9H_2O$ of a purity of 99.9% was dissolved in ethanol, and then ZnO powder (99.999%) was added in the solution. The suspension was stirred while heated to evaporate the ethanol until dryness. The uniformly mixed powder was then pressed into disks and sintered on platinum plates in air at 1273 K for 3 h. Commercially available ^{111}In HCl solution was added in droplets onto the sintered disks. The initial concentration of ^{111}In ions doped in the sample was typically ~100 ppt. After the disks were dried up by heat, they again underwent heat treatment in air at 1373 K for 2 h. Following the doping of ^{111}In, the disks were separately ground into powder. A TDPAC measurement was performed for one of these powder samples prepared in air. The rest of the powder samples were separately sealed in quartz tubes in vacuum and 1123-K isothermal annealing was performed one by one for different annealing times (3600~90000 s) for the investigation of annealing-time dependence of the thermal stability of Al and In impurities in ZnO. The TDPAC measurements were carried out at room temperature for the 171-245 keV cascade γ rays of the ^{111}In($\rightarrow^{111}$Cd) probe with the intermediate state of I = 5/2 having a half-life of 85.0 ns.

2-2 Isochronal Annealing

Following the examination of the annealing-time dependence of the locally-

associated In-Al structure, the temperature dependence of the local structure was examined. The experimental procedure is schematized in Fig. 25.

The preparation procedure for the disks of 100-ppm Al-doped ZnO and the doping method of ^{111}In are the same as those for the experiments described in the previous section. Following the doping of ^{111}In, the disks were separately ground into powder. A TDPAC measurement was performed for one of these powder samples prepared in air. The rest of the powder samples were separately sealed in quartz tubes in vacuum and 24-h isochronal annealing was performed one by one at different temperatures (873~1148 K) for the investigation of annealing-temperature dependence of the thermal stability of Al and In impurities in ZnO. The TDPAC measurements were carried out at room temperature for the 171-245 keV cascade γ rays of the ^{111}In($\rightarrow^{111}$Cd) probe with the intermediate state of I = 5/2 having a half-life of 85.0 ns.

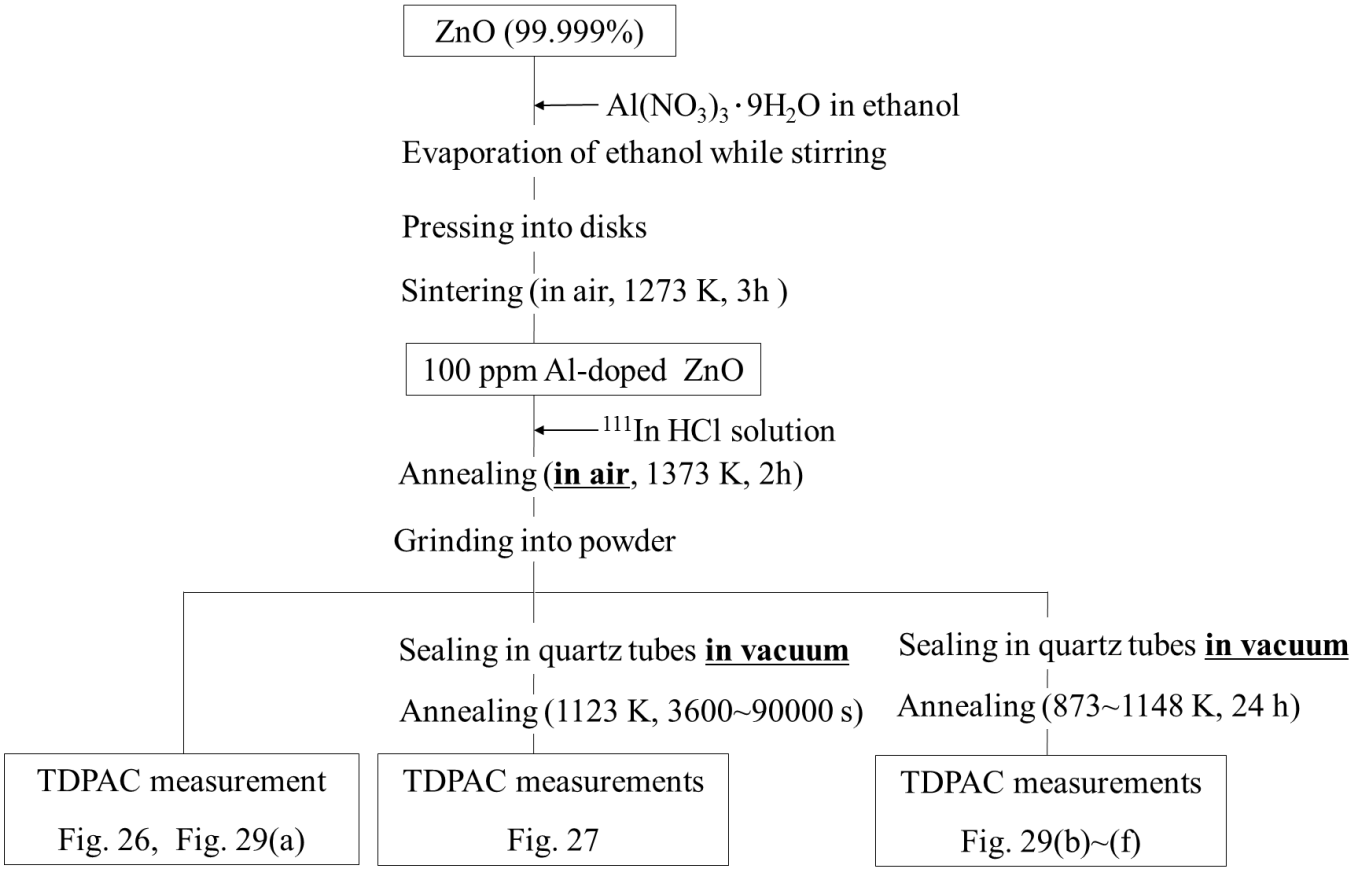

Fig. 25 Experimental procedure of sample preparation and TDPAC measurements for 100 ppm Al-doped ZnO

Chapter 3 Results and Discussion

3-1 Result of TDPAC Measurements

3-1-1 100-ppm Al-Doped ZnO Prepared by Isothermal Annealing

The stability of the locally-associated Al and In in annealing process for various annealing-times(3600 – 90000 s) in vacuum was inestigated. Figure 26 shows the spectrum obtained for the sample prepared by heat treatment in air. Figures 27(a) to 27(f) are the TDPAC spectra for the samples heat-treated in vacuum at 1123 K for various annealing times after the doping of the ^{111}In probe in air. The parameter values obtained by the least squares fits with Eq. (9) are listed in Table 5.

The spectrum in Fig. 26 was obtained in the same procedure taken in our previous work, which is described in Section 1-3 of PART I. The reproducibility was confirmed by the parameter values for the predominant component as listed in Table 5. In Fig. 27(a), however, another component exhibiting a small undulation at around 200 ns slightly appeared after the heat treatment in vacuum at 1123 K for 3600 s (Component I). It has already been known from a previous TDPAC study[21] that Component I corresponds to the ^{111}In($\rightarrow^{111}$Cd) probe occupying defect-free substitutional Zn site; the EFG value ($1.7(3)\times10^{21}$ V/m^2) obtained from the fit to the spectrum shows good agreement with theoretical values estimated for a Cd^{2+} ion residing at the defect-free Zn site (1.565×10^{21} and 1.68×10^{21} V/m^2).[23, 24] Component I becomes more visible with increasing annealing time after the heat treatment in vacuum for 90000 s as shown in Fig. 27(f). This observation is depicted in Fig. 28, showing the fractions of Components I and II (called f_{I} and f_{II}, respectively) as functions of annealing time. We can clearly see the trend of the fractional shift from Component II to I as the annealing time increases.

3-1-2 100-ppm Al-Doped ZnO Prepared by Isochronal Annealing

We obtained the room-temperature TDPAC spectrum for 100-ppm Al-doped ZnO heat treated in air at 1373 K for 2 h as shown in Fig. 29(a) to confirm the reproducibility of the spectral pattern shown in Fig. 11(e). Figures 29(b) to 29(f) are the TDPAC spectra for the samples heat-treated in vacuum at various temperatures. The parameter values were obtained by least squares fits with Eq. (9) again, and listed in Table 6. As already discussed in Subsection 3-1-1, the component showing a damping structure seen in Fig. 29(a) corresponds to the ^{111}Cd(←^{111}In) probe associated with Al ions. In Fig. 29(b), as shown by a small undulation at around 200 ns, another structure slightly appeared after the heat treatment in vacuum at 873 K. It has already been known from a previous TDPAC study[21] that Component I corresponds to the ^{111}Cd(←^{111}In) probe occupying the defect-free substitutional Zn site. Component I becomes more visible with increasing annealing temperature, and eventually becomes predominant at the annealing temperature of 1148 K, indicating its fraction of 87(1)%. This observation suggests that the dissociation of Al and In proceeded to near completion, and most of the probe ions eventually reside at defect-free Zn sites by the heat treatment in vacuum at 1148 K.

The fractions of Component I and Component II are plotted as functions of annealing temperature in Fig. 30. We can clearly see increasing trend of the fraction of Component I with increasing annealing temperature, showing the enhancement of the dissociation process of Al and In at higher temperature.

Table 5 Parameter values obtained by least-squares fits on the TDPAC spectra of ^{111}In(→^{111}Cd) in 100-ppm Al-doped ZnO.

Corresponding spectrum in Figs. 26 and 27	Annealing time (s)	Component	V_{zz} (10^{21} V/m^2)	η	δ (%)	Fraction (%)
Fig. 26	—[a]	II	8.0(13)	0.55(3)	46(2)	100(1)
Fig. 27(a)	3600	II	8.0(13)	0.55(3)	32(3)	80(3)
		I	1.7(3)	0	0	20(2)
Fig. 27(b)	6000	II	8.4(14)	0.55(3)	31(4)	63(3)
		I	1.7(3)	0	0	37(2)
Fig. 27(c)	10800	II	8.5(14)	0.55(3)	30(3)	63(2)
		I	1.7(3)	0	0	37(2)
Fig. 27(d)	25200	II	8.5(14)	0.55(3)	31(5)	56(3)
		I	1.7(3)	0	0	44(2)
Fig. 27(e)	50400	II	8.6(15)	0.55(3)	22(6)	44(3)
		I	1.7(3)	0	0	56(3)
Fig. 27(f)	90000	II	8.3(14)	0.55(3)	24(7)	38(3)
		I	1.7(3)	0	0	62(3)

[a] The sample as prepared in air. See the text and Fig. 25 for the sample preparation.

Table 6 Parameter values obtained by least-squares fits on the TDPAC spectra of ^{111}In(→^{111}Cd) in 100-ppm Al-doped ZnO.

Corresponding spectrum in Fig. 29	Annealing temperature (K)	Component	V_{zz} (10^{21} V/m^2)	η	δ (%)	Fraction (%)
(a)	—[a]	II	8.8(14)	0.55(3)	36(2)	96(1)
(b)	873	II	7.9(13)	0.55(3)	38(2)	87(2)
		I	1.7(3)	0	0	6(2)
(c)	1023	II	8.3(13)	0.55(3)	26(2)	72(2)
		I	1.7(3)	0	0	19(2)
(d)	1073	II	8.2(13)	0.55(3)	32(2)	66(2)
		I	1.7(3)	0	0	27(2)
(e)	1123	II	7.8(13)	0.55(3)	29(4)	36(2)
		I	1.7(3)	0	0	52(2)
(f)	1148	I	1.7(3)	0	0	87(1)

[a] The sample as prepared in air. See the text and Fig. 25 for the sample preparation.

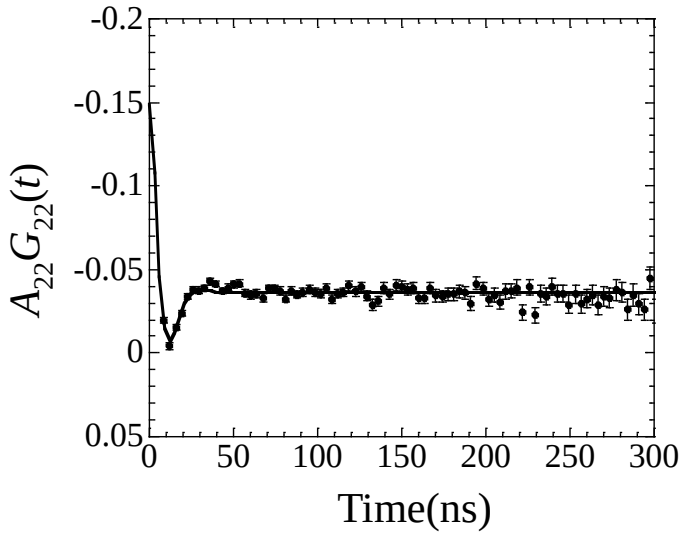

Fig. 26 TDPAC spectrum for 100-ppm Al-doped ZnO annealed in air at 1373 K. TDPAC measurement was performed at room temperature.

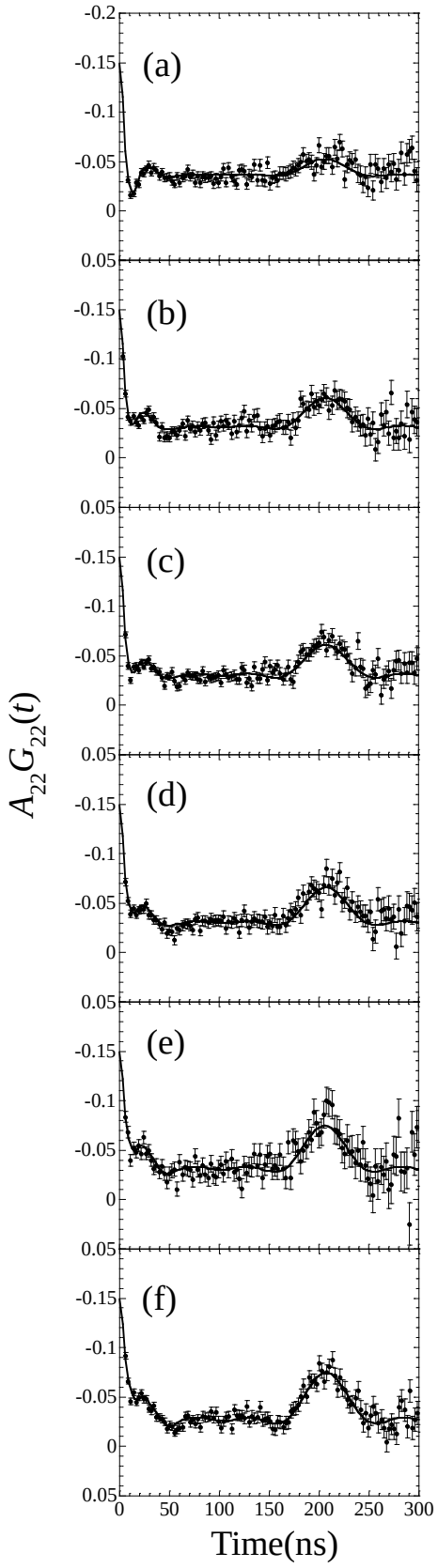

Fig. 27 TDPAC spectra for 100-ppm Al-doped ZnO subsequently annealed in vacuum. Annealing times are (a) 3600 s, (b) 6000 s, (c) 10800 s, (d) 25200 s, (e) 50400 s, and (f) 90000 s. TDPAC measurements were performed at room temperature.

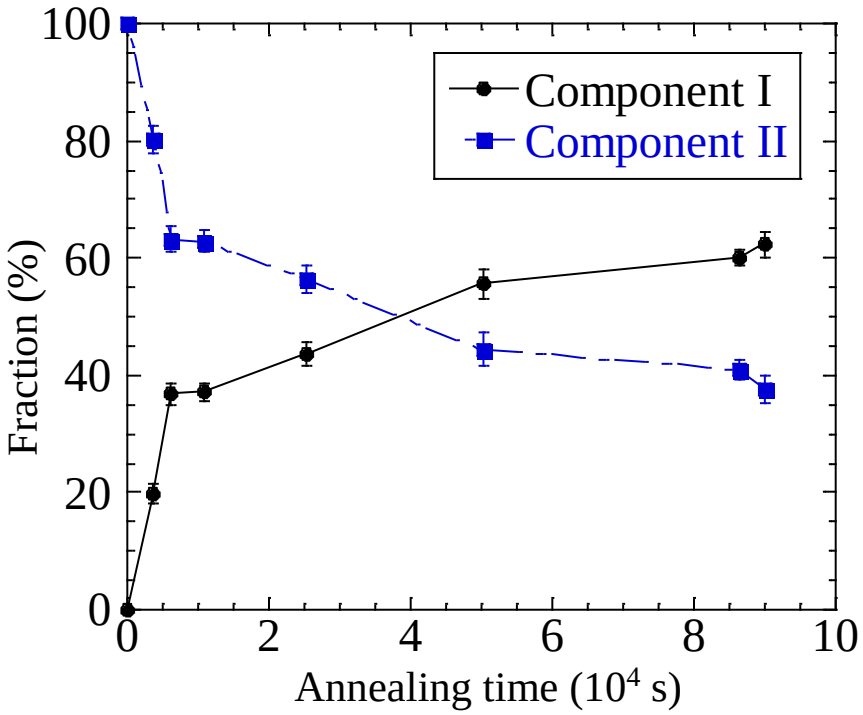

Fig. 28 Fractions of ^{111}In in substitutional Zn site (●) and ^{111}In associated with Al (■) as functions of annealing time. Annealing temperature is 1123 K.

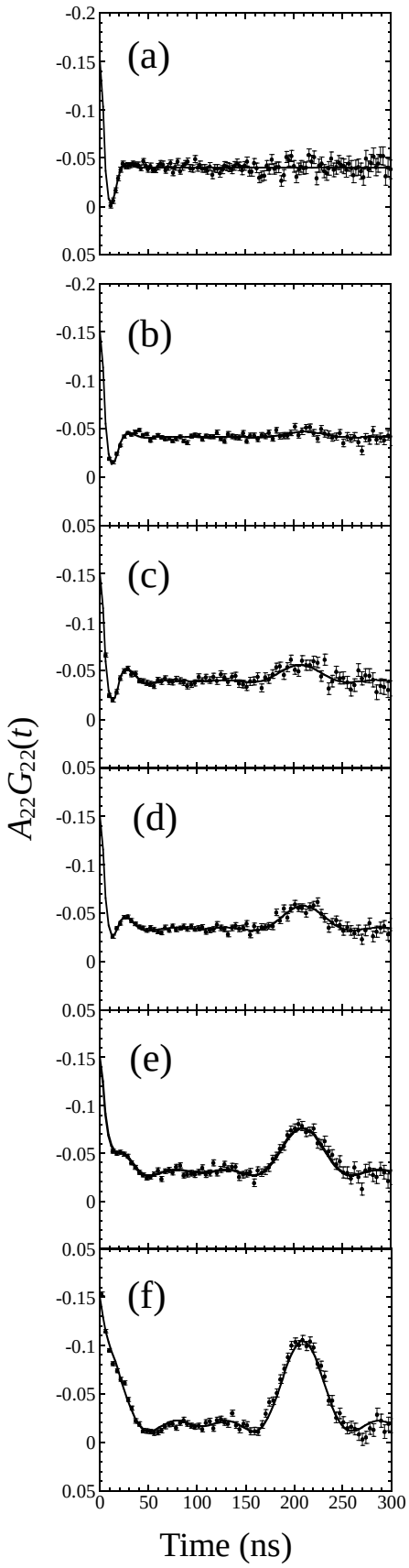

Fig. 29 (a) TDPAC spectrum of ^{111}In($\rightarrow^{111}$Cd) in 100-ppm Al-doped ZnO annealed in air at 1373 K. (b)-(f) TDPAC spectra of ^{111}In($\rightarrow^{111}$Cd) in 100-ppm Al-doped ZnO subsequently annealed in vacuum for 24 h after the measurement of the spectrum in (a). Annealing temperatures are (b) 873 K, (c) 1023 K, (d) 1073 K, (e) 1123 K, and (f) 1148K. All the TDPAC measurements were performed at room temperature.

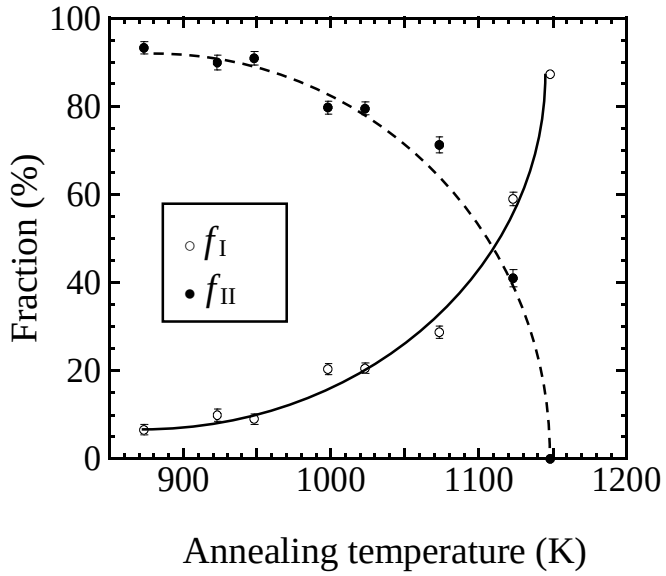

Fig. 30 Fractions of Component I (f_{I}) and Component II (f_{II}) as functions of annealing temperature for annealing time 24 h. The solid and dashed lines are guides to the eye.

3-2 Discussion

3-2-1 Rate Constant

The annealing-time dependence of f_{II} is shown in Fig. 31 on a logarithmic scale. The f_{II} values are exponentially reduced with increasing annealing time, suggesting that this dissociation reaction proceeds through the first-order kinetics. They were thus fitted with the following relation:

$$f_{II}(t) = f_{II}(0)\, e^{-kt}. \quad (12)$$

The data points indicated by solid squares are reproduced well by the fit, and the rate constant, k, was evaluated to be $6.0(6)\times10^{-6}$ s^{-1} for the annealing-time range. However, the data obtained by a short time annealing (t = 3600 s) apparently deviates from the line. An interpretation of this deviation is that part of the ^{111}In probes loosely bound to the Al aggregation is immediately detrapped to diffuse into the bulk. This process should be controlled by another kinetics with a larger rate constant as assumed by the dashed line.

3-2-2 Activation Energy

For the first-order reaction of the dissociation process of In and Al ions, the activation energy can be estimated from the temperature dependence of the rate constant k. We thus obtained the k values at different temperatures as well in a similar way[39-41]. Their temperature variation is plotted in Fig. 32. A least-squares fit to the k values was then carried out with the following Arrhenius equation:

$$k = \nu_0 \exp\left(\frac{-E_a}{k_B T}\right), \qquad (13)$$

and the activation energy, E_a, was evaluated to be 0.72 (6) eV. Taking into consideration a reported activation energy of the thermal diffusion of In impurities in ZnO (2.69 (18) eV)[43], we can exclude a possibility that the present E_a value is of the migration energy of the ^{111}In probe in the bulk ZnO. Because the dissociation process of the ^{111}In probe and Al would be induced by the formation of oxygen vacancies as discussed above, we suggest that the observed E_a is related to the formation of oxygen vacancies at grain boundaries in polycrystalline Al-doped ZnO sample. This interpretation is supported by the fact that the present E_a value shows good agreement with the theoretical ones calculated for the formation energy of oxygen vacancies in ZnO (0.85 and 1.0 eV)[38, 44-46].

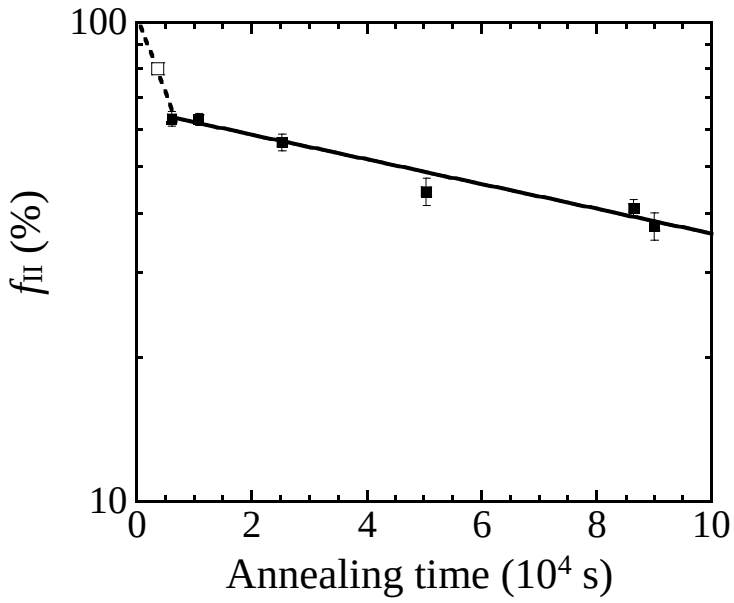

Fig. 31 Annealing-time dependence of the fraction of Component II (f_{II}) observed for the samples prepared by the isothermal annealings at 1123 K. The data were fitted with Eq. (12).

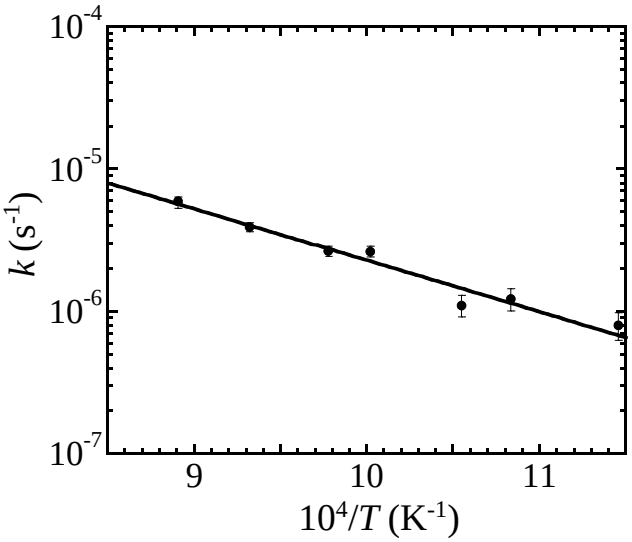

Fig. 32 Temperature dependence of the rate constant, *k*. An Arrhenius equation, Eq. (13), was used for the fit[42].

Chapter 4 Summary of PART II

In PART II, TDPAC measurements were performed for 100-ppm Al-doped ZnO prepared by isothermal and isochronal annealings in vacuum, and association and dissociation reactions of the dilute Al and ^{111}In in ZnO were quantitatively discussed based on the rate constant and the activation energy for the dissociation reactions. As described in Chapter 1, Al and In impurities associate with each other by their thermal diffusion in air, however, in high-temperature vacuum, the ^{111}In probe can be detrapped from the Al aggregations resulting in substitution at defect-free Zn sites.

For more quantitative discussion on these reactions, we performed isothermal annealing in vacuum for ZnO doped with Al and ^{111}In; subsequent TDPAC measurements have revealed that the dissociation reactions are controlled by the first-order rate law. Furthermore, the activation energy E_a for the dissociation process was evaluated from the temperature variation of the rate constants k to be 0.72(6) eV. We suggest based on the proposed mechanism of the dissociation process of the impurities that this E_a is related to the formation energy of oxygen vacancies in Al-doped ZnO sample, which is supported by good agreement with theoretical values (0.85 and 1.0 eV).

REFERENCES

[1] S. J. Pearton, D. P. Norton, K. Ip, Y. W. Heo, and T. Steiner: Prog. Mater. Sci. **50**, 293, (2005).

[2] Z. L. Wang: J. Phys.: Condens. Matter **16**, R829, (2004).

[3] I. A. Ezenwa: Res. J. Chem. Sci. **2(3)**, 26, (2012).

[4] Y. Teow, P. V. Asharani, M. P. Hande, and S. Valiyaveettil: Chem. Commun. **47**, 7025 (2011)

[5] A. V. Kachynski, A. N. Kuzmin, M. Nyk, I. Roy, and P. N. Prasad: J. Phys. Chem. C **112**, 10721 (2008)

[6] R. Dingle: Phys. Rev. Lett. **23**, 579, (1969).

[7] Y. Fujishiro, M. Miyata, M. Awano, and K. Maeda: J. Am. Ceram. Soc. **86**, 2063 (2003).

[8] C. Y. Hsua, T. F. Ko, and Y. M. Huang: J. Eur. Ceram. Soc. **28**, 3065 (2008).

[9] A. Sedky, AymanAl-Sawalha, and A. M. Yassin: Phys. B **404**, 3519 (2009).

[10] L. Han, L. T. Hung, N. Nong, N. Pryds, and S. Linderoth, J. Electron: Mater. **42**, 1573, (2013).

[11] Y. Takeda, K. Nomura, H. Ohta, H. Yanagi, T. Kamiya, M. Hirano, and H. Hosono: Thin Solid Films **486**, 28, (2005).

[12] M. S. Park and B. I. Min: Phys. Rev. B **68**, 224436, (2003).

[13] X. C. Liu, E. W. Shi, Z. Z. Chen, H. W. Zhang, B. Xiao, and L. X. Song: Appl. Phys. Lett. **88**, 252503, (2006).

[14] Ü. Özgür, Ya. I. Alivov, C. Liu, A. Teke, M. A. Reshchikov, S. Doğan, V. Avrutin, S.-J. Cho, and H. Morkoç: J. Appl. Phys. **98**, 041301, (2005).

[15] L. Schmidt-Mende and J. L. MacManus-Discoll: Mater. Today **10**, 40 (2007).

[16] Z. Deng, C. Huang, J. Huang, M. Wang, H. He, H. Wang, and Y. Cao: J. Mater.

Sci.: Mater. Electron. **21**, 1030, (2010).

[17] Y. Yang, X. Zeng, Y. Zeng, L. Liu, and Q. Chen: Appl. Surf. Sci. **257**, 232, (2010).

[18] B. J. Babu, A. Maldonado, S. Velumani, and R. Asomoza: Mter. Sci. Eng. B **174**, 31, (2010).

[19] Y. S. Kim and W. P. Tai: Appl. Surf. Sci. **253**, 4911, (2007).

[20] J. G. Lu, Z. Z. Ye, Y. J. Zeng, L. P. Zhu, L. Wang, J. Yuan, B. H. Zhao, and Q. L. Liang: J. Appl. Phys. **100**, 073714, (2006).

[21] W. Sato, Y. Itsuki, S. Morimoto, H. Susuki, S. Nasu, A. Shinohara, and Y. Ohkubo: Phys. Rev. B, **78**, 045319, (2008).

[22] T. Butz: Hyp. Int. **52**, 189, (1989).

[23] H. E. Mahnke: Hyp. Int. **49**, 77, (1989).

[24] H. Frauenfelder and R. M. Steffen , in *(A) Angular Correlations* in *Angular Distribution of Nuclear Radiation,* edited by K. Siegbahn, *α*-, *β*-, and *γ-Ray Spectroscopy* (North-Holland, Amsterdam, 1974), Vol. 2.

[25] *Table of Isotopoes,* edited by R. B. Firestone and V. S. Shirley (Wiley, New York, 1996), Vol. 1, 8th ed.

[26] W. Sato, Y. Komeno, M. Tanigaki, A. Taniguchi, S. Kawata, and Y. Ohkubo: J. Phys. Soc. Jpn. **77**, 105001, (2008).

[27] U. Bäverstam, R. Othaz, N. Sousa, and B. Ringsröm: Nucl. Phys. A **186**, 500, (1972).

[28] A. Abragm and R. V. Pound: Phys. Rev. B, **92**, 943, (1953).

[29] Y. Abreu, C. M. Cruz, P. Van Espen, C. Pérez, I. Piñera, A. Leyva, and A. E. Cabal: Solid State Commun. **152**, 399, (2012).

[30] E. L. Muñoz, M. E. Mercurio, M. R. Corderio, L. F. D. Pereira, A. W. Carbonari,

and M. Renteria: Physica B **407**, 3121, (2012).

[31] W. Sato, S. Komatsuda, and Y. Ohkubo, Phys. Rev. B **86**, 235209, (2012).

[32] CRC Handbook of Chemistry and Physics 79th Edition

[33] T. G. G. Maffeis, M. W. Penny, J. D. W. Garbutt, and S. P. Wilks: Phys. Status Solidi A **207**, 282, (2010).

[34] G. J. Fanga, D. Li, and B. L. Yao: Thin Solid Films **418**, 156, (2002).

[35] Lennon, R. B. Tapia, R. Kodama, Y. Chang, S. Sivananthan, and M. Deshpande: J. Elec. Mater. **38**, 1568, (2009)

[36] G. J. Fang, D. J. Li, and B. L. Ya: Phys. Status Solidi (a) **193**, 139, (2002).

[37] T. Ogawa, A. Kuwabara, C. A. J. Fisher, H. Moriwake, K. Matsunaga, K. Tsuruta, and S. Kitaoka: Acta Mater. **69**, 365, (2014).

[38] S. Lany and A. Zunger: Phys. Rev. Lett. **98**, 045501, (2007).

[39] U. Wahl, A. Vantomme, and G. Langouche: Phys. Rev. Lett. **84**, 1495, (2000).

[40] D. A. Brett, R. Dogra, A. P. Byne, J. Mestnik-Filho, and M. C. Ridgway: Phys. Rev. B **72**, 193202, (2005).

[41] The k values for the dissociation reaction at respective temperatures should also be determined by the same measure taken for the 1123-K data shown in Fig. 31. Because the relevant reaction proceeds slower at lower temperatures in a time scale of several weeks typically, however, the radioactive probe ^{111}In ($T_{1/2}$ = 2.8 d) needs to be doped in a considerable amount in advance; which causes a great deal of other unwanted impurities to be mixed in. Therefore, we examined the applicability of a simpler way to estimate the k value with $f_{II}(0)$ and a sole $f_{II}(t)$ obtained by the 24-h annealing according to Eq. (12). As read from Fig. 31, this approximation, with the extrapolated value of $f_{II}(0)$ = 66%, goes well for the 1123-K data giving $k = 5.6(6)\times10^{-6}$ s^{-1}, which shows good

agreement with that evaluated by the fit. As regards the $f_{II}(0)$ values for the rest of the data at lower temperatures, we assumed $f_{II}(0) = 100\%$. This assumption is based on the experimental fact that $f_{II}(t)$ values hardly reach 66% even at t = 86400 s (24 h) at temperatures lower than 1123 K. It is thus reasonable to approximately regard the low-temperature thermal reaction as proceeding on a single first-order kinetics.

[42] The k value for the 1148-K data is not plotted in the figure because of lack of reliability; the relevant $f_{II}(t)$ values obtained by the isothermal annealing at this high temperature are considerably dispersed from such a line as expected for a uniform annealing-time dependence shown in Fig. 31.

[43] I. Sakaguchi, D. Park, Y. Takata, S. Hishita, and N. Ohashi: Nucl. Instr. Meth. Phys. Res. **206**, 153, (2003).

[44] F. Oba, A. Togo, and T. Isao: Phys. Rev. B **77**, 245202, (2008).

[45] T. R. Paudel and W. R. L. Lambrecht: Phys. Rev. B, **77**, 205202 (2008)

[46] S. J. Clark, J. Robertson, S. Lany, and A. Zunger: Phys. Rev. B, **81**, 115311 (2010)

APPENDIX

A1

Absorption of ^{111}In to $ZnAl_2O_4$ Observed by TDPAC Spectroscopy

A1-1 Introduction

As described in Chapter 2 of PART I, it is suggested that the ^{111}In($\rightarrow^{111}$Cd) probe is locally associated with $ZnAl_2O_4$ even at as extremely low concentration as 0.01 ppm of Al. For the corroboration of the inference, the bonding state of $ZnAl_2O_4$ and ^{111}In ions in ZnO was examined. In the present work, for investigating the interacting nature between the ^{111}In($\rightarrow^{111}$Cd) probe and $ZnAl_2O_4$, a TDPAC spectrum was obtained for the ^{111}In($\rightarrow^{111}$Cd) probe doped in $ZnAl_2O_4$ polycrystal.

A1-2 Experiment

Experimental procedure is schematized in Fig. A1. Commercially available $ZnAl_2O_4$ polycrystal powder was pressed into a disk and sintered on a platinum plate in air at 1273 K for 3 h. Commercially available ^{111}In HCl solution was then added in droplets onto the sintered disk. The initial concentration of ^{111}In ions doped in the sample was typically ~100 ppt. After the disk was dried up by heat, it again underwent heat treatment in air at 1373 K for 2 h. Following the doping of ^{111}In, the disk was separately ground into powder and sealed in quartz tube. The TDPAC measurement was carried out at room temperature for the 171-245 keV cascade γ rays of the ^{111}In($\rightarrow^{111}$Cd) probe with the intermediate state of I = 5/2 having a half-life of 85.0 ns.

A1-3 Results and Discussion

Figure A2 shows the TDPAC spectrum for the $ZnAl_2O_4$ observed at room temperature. The parameter values obtained by a least squares fit with Eq. (9) are listed in Table A1. For comparison, parameter values of 10 at.% Al-doped ZnO are cited in Table A1 from Table 2. As for the $ZnAl_2O_4$, the oscillating pattern reproducible with a single component is not clearly discernible due to the damped structure reflecting a wide distribution of the field at the probe. The other hyperfine interaction parameters (V_{ZZ}, f) from the spectrum of $ZnAl_2O_4$ show the same values with those of a Al-doped ZnO sample within uncertainties. The δ value for the sample of $ZnAl_2O_4$ is quite large as listed in Table A1. The widely distributed EFG may arise from the probes adsorbed to various grain boundaries of $ZnAl_2O_4$ as schematized in Fig. A3. (If the $^{111}In(\rightarrow^{111}Cd)$ probe ions are located at the specific site (such as the substitutional Al site or an interstitial site), the δ value should be small.) It is thus suggested that the strong interaction between ^{111}In and $ZnAl_2O_4$ is not of chemical bonding, but of undefined physical adsorption.

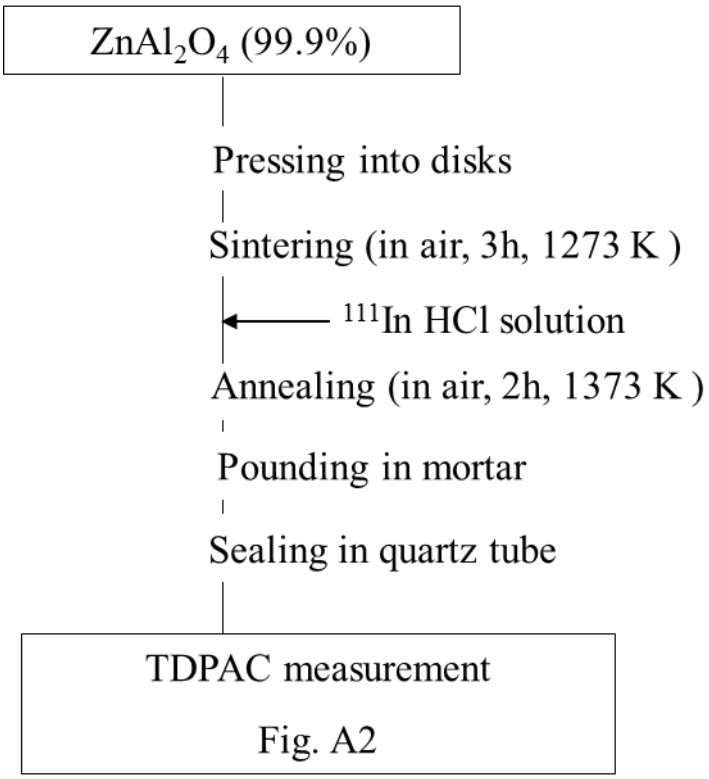

Fig. A1 Experimental procedure of sample preparation and TDPAC measurements for $ZnAl_2O_4$.

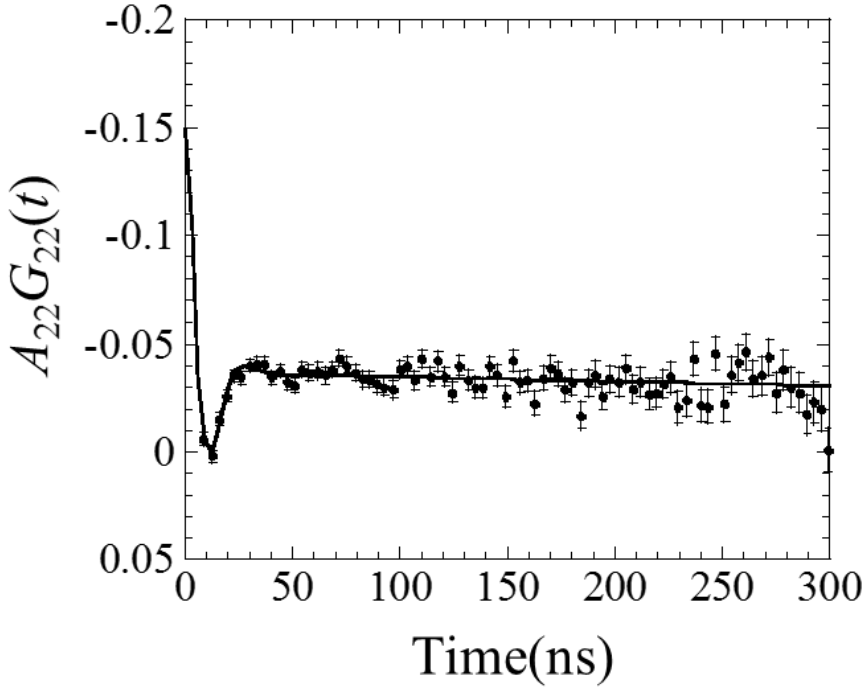

Fig. A2 TDPAC spectrum of ^{111}In(→^{111}Cd) in $ZnAl_2O_4$ measured at room temperature.

Table A1 Parameter values obtained by least-squares fits on the TDPAC spectra of $^{111}In(\rightarrow^{111}Cd)$ in $ZnAl_2O_4$ and in 10 at.% Al-doped ZnO.

Sample	V_{zz} ($10^{21}V/m^2$)	δ (%)	Fraction (%)
$ZnAl_2O_4$	8.7(15)	38(3)	99(3)
10 at.% Al-doped ZnO (Cited from Table 2)	8.2(13)	42(3)	99(2)

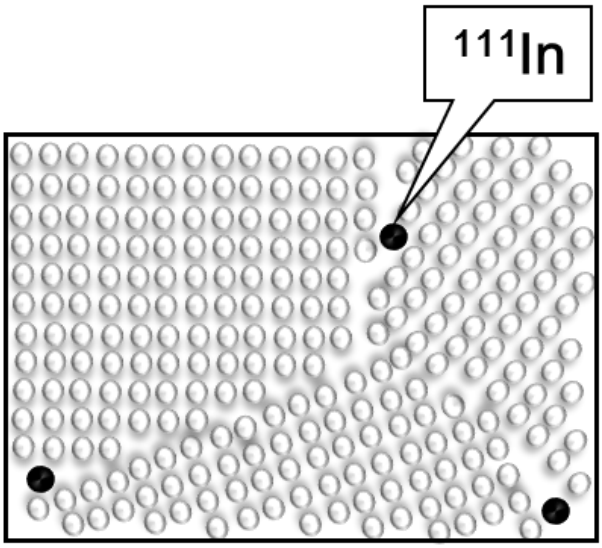

Fig. A3 Schematic diagram of adsorption to ^{111}In to grain boundaries of $ZnAl_2O_4$

A2

Distribution of Electric Quadrupole Frequency

Figure A4 shows simulated TDPAC spectra for I = 2/5 and ω_Q= 25.2 Mrad/s. Gaussian distribution with its relative width δ is expressed as follows:

$$\delta = \frac{\sigma}{\omega_\theta}.$$

Here, σ is Gaussian distribution width, and ω_0 is the centroid of the nuclear quadrupole frequency.

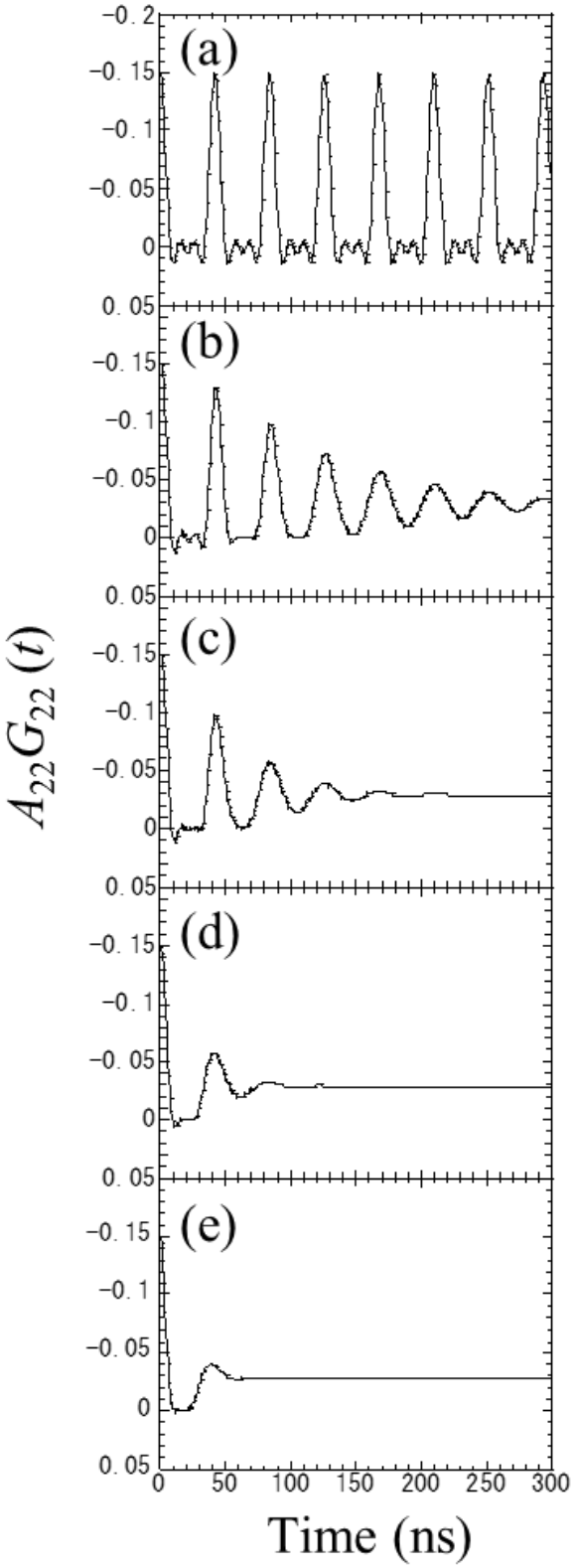

Fig. A4 Simulated TDPAC spectra for I = 2/5 and ω_Q= 25.2 Mrad/s. Different distribution δ of the electric quadrupole frequencies ω_Q are assumed for each spectrum: (a) 0%, (b) 5%, (c) 10%, (d) 20%, and (e) 30%.

A3

Atmosphere Dependence of Local Fields in Al-doped ZnO Investigated by the TDPAC Method with ^{111m}Cd($\rightarrow^{111}$Cd) Probe

A3-1 Introduction

It was proposed in Chapter 4 of PART I that the bound state of ^{111}In and $ZnAl_2O_4$ grains is dissociated by heat-treatment in vacuum by triggered the formation of oxygen vacancies in the vicinity of locally-associated In-Al structures. In order to provide insight into the effect of the heat-treatment condition, in this section, the structural change for Al-doped ZnO prepared by long-heating in vacuum was investigated by the TDPAC method with the ^{111m}Cd($\rightarrow^{111}$Cd) probe in 0.01 at.% Al-doped ZnO .

A3-2 Experiment

Experimental procedure is schematized in Fig. A5. 0.01 at.% Al-doped ZnO disk samples were prepared in the same way as that described in Section 1-2 of PART I. After the preparation, the disks were separately ground into powder and sealed in quartz tubes in vacuum, respectively. They underwent further heat treatment in vacuum at 1273 K for 100 h. About 3 mg of CdO enriched with ^{110}Cd was irradiated with thermal neutrons in a pneumatic tube at Kyoto University Reactor, and radioactive ^{111m}Cd was generated by ^{110}Cd(n,γ)^{111m}Cd reaction. The neutron-irradiated CdO powder was then

separately added into the long-heated samples and mixed again in a mortar for 20 min. Each of the mixtures was pressed into disks. The samples were sintered in different atmosphere: one was in air and the other in vacuum at 1373 K for 45 min. TDPAC measurements were carried out for the ^{111m}Cd($\rightarrow^{111}$Cd) probe on the 151-245 keV cascade γ rays with the intermediate state of I= 5/2 having a half-life of 85.0 ns.

A3-3 Results and Discussion

Figure A6 shows the TDPAC spectra of ^{111m}Cd($\rightarrow^{111}$Cd) probe in 0.01 at.% Al-doped ZnO annealed (a) in vacuum and (b) in air. The value of the electric field gradient at the probe nucleus is $1.7(3)\times10^{21}$ Vm^{-2} for both spectra in Fig. A6(a) and A6(b), which suggests that the ^{111m}Cd($\rightarrow^{111}$Cd) probe resides at the defect-free substitutional Zn site regardless of the presence of Al impurities in the system. With respect to Fig. A6(a), the prominent spectral damping appears as a result of large distribution of the quadrupole frequency δ(= 8.9 (6)%). The large δ value could be attributed to the remains of oxygen vacancies around the probe formed by the long annealing process in vacuum. On the otherhand, the damping effect in Fig. A6(b) is not as prominent as that in the spectrum in Fig. 6(a). This is due to the refilling of oxygen atoms by the annealing in air. Schematic views of the dispersion state of ^{111m}Cd ions is shown in Fig. A7 for better understanding. From these observations, it was confirmed that the formation of oxygen vacancies proceeds during annealing process at a lower partial pressure of atmospheric oxygen in ZnO system.

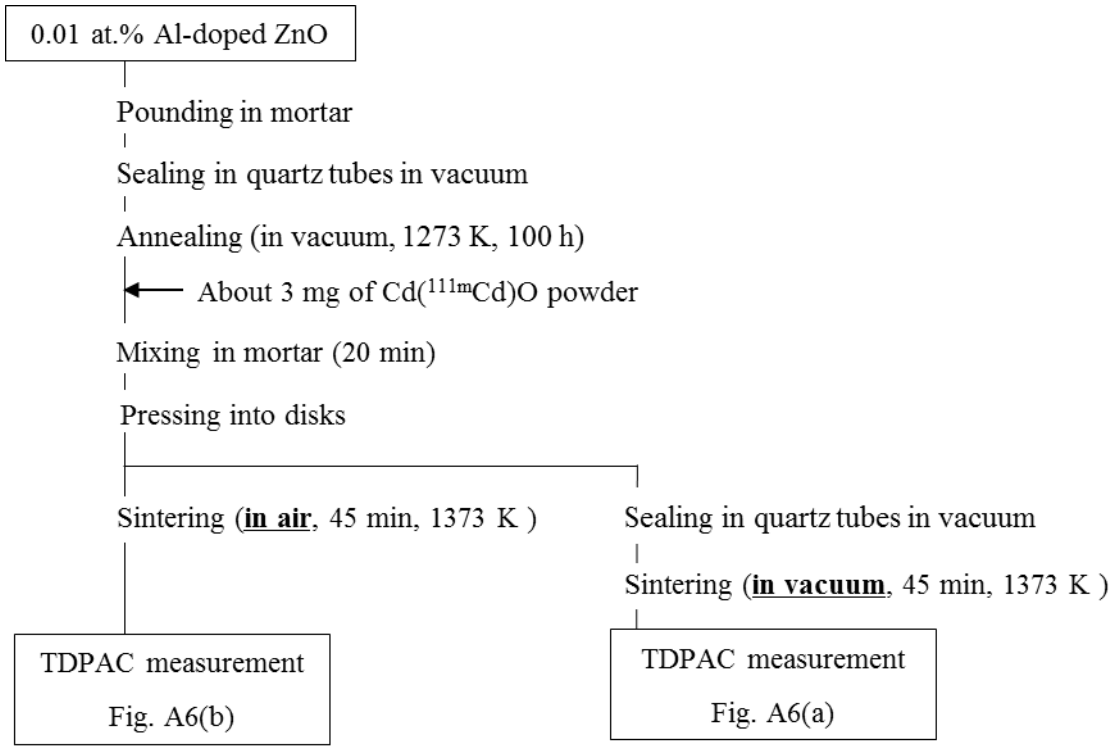

Fig. A5 Experimental procedure of sample preparation and TDPAC measurements of ^{111m}Cd($\rightarrow^{111}$Cd) in 0.01 at.% Al-doped ZnO.

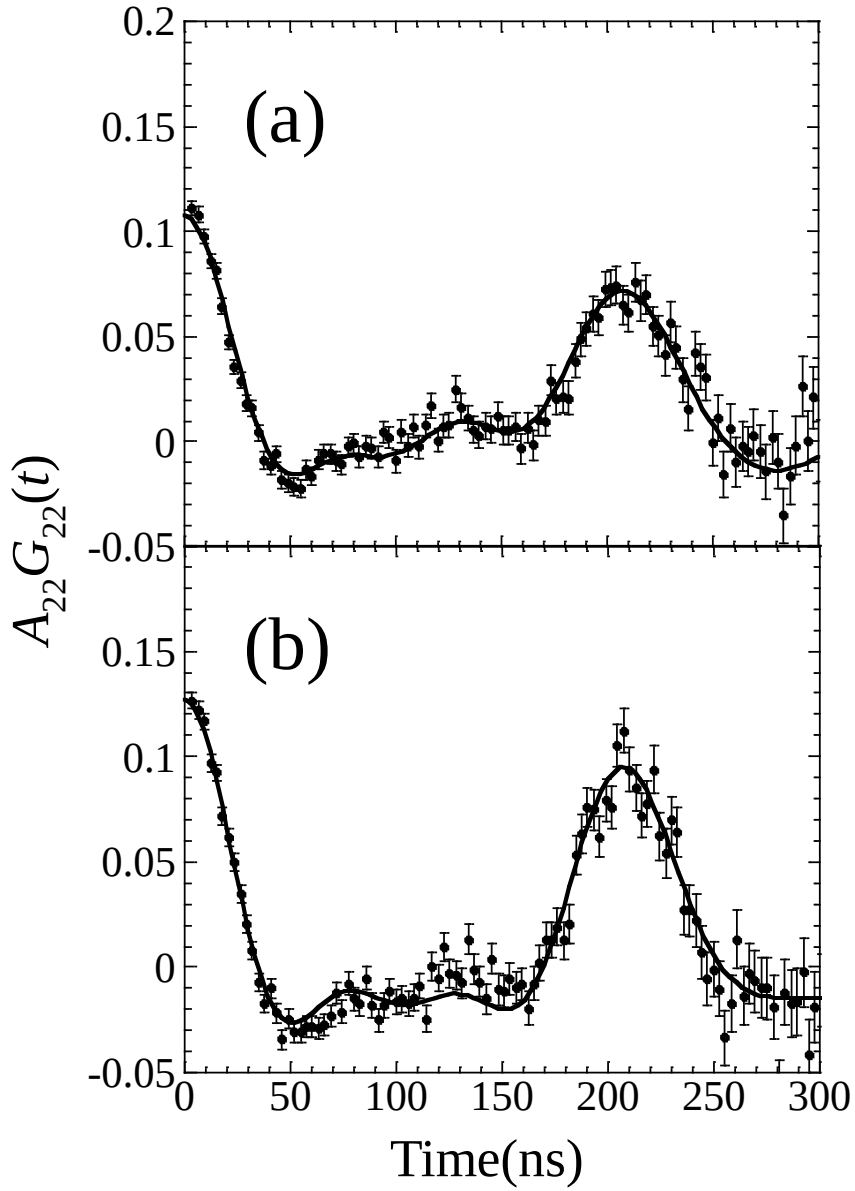

Fig. A6 TDPAC spectra of ^{111m}Cd($\rightarrow^{111}$Cd) in 0.01 at.% Al-doped ZnO annealed (a) in vacuum and (b) in air.

Table A2 Parameter values obtained by least-squares fits on the TDPAC spectra of ^{111m}Cd($\rightarrow^{111}$Cd) in 0.01 at.% Al-doped ZnO.

Corresponding spectrum	Heat-treatment condition	Component	Site assignment	V_{zz} (10^{21}V/m^2)	δ (%)
Fig. A6(a)	in vacuum	I	substitutional Zn site	1.7(3)	8.9(6)
Fig. A6(b)	in air	I	substitutional Zn site	1.7(3)	7.3(5)

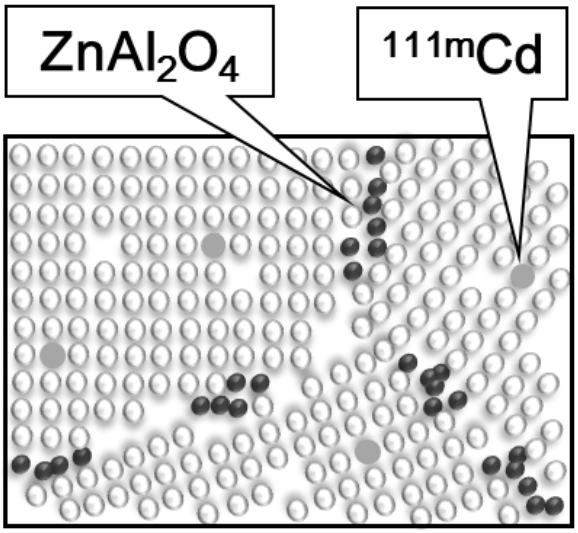

Fig. A7　Schematic diagram of the dispersion state of ^{111m}Cd

A4

Electric Resistivity of undoped and Al-doped ZnO Samples

A4-1 Introduction

As discussed in PART I, the findings for Al-doped ZnO in this studies are as follows: (1) in spite of the large concentration gap, there is not a noticeable difference between 10^{-6} at.% Al-doped ZnO and 10 at.% Al-doped ZnO in terms of Al local structures, and (2) Al and In are strongly bound to each other in ZnO during heat treatment "in air," whereas in high-temperature ''vacuum'', dissociation reaction of Al and In triggered by the formation of oxygen vacancies in the vicinity of the locally-associated In-Al structure was observed.

Electric properties are affected by the physical and chemical states of defects such as impurity ions and vacancies. It is then essential to clarify the relation between local structure in ZnO and the electric property for its application to semiconductor devices. Therefore, in order to understand the effect of local structures formed by impurities, electric resistivities of synthesized Al-doped ZnO samples were measured. In this section, the concentration dependence and atmosphere dependence of the resistivity of Al-doped ZnO sample are discussed.

A4-2 Experiment

Experimental procedure is schematized in Fig. A8. For the investigation of the

Al concentration dependence of electric resistivity, Al-doped ZnO powder samples were prepared in the same way as that described in Section 1-2 of PART I. For the investigation of the atmosphere dependence, undoped and 0.01 at.% Al-doped ZnO disks were prepared. A four-terminal resistivity measurement was performed for one of these disks prepared in air. The rest of the disks were annealed in vacuum at 1148 K for 24 h and in argon at 1273 K for 24 h, respectively. Four-terminal resistivity measurements were then performed for these samples.

A4-3 Results and Discussion

Table A3 shows the concentration dependence of electric resistivity for Al-doped ZnO. In spite of the large concentration gap, the difference of all resistivity values are within one order of magnitude. Namely, there is no noticeable relation between Al concentration and resistivity, which is consistent with the findings in Chapter 1of PART I that even ppm-level dilute Al impurities locally associate with each other to form $ZnAl_2O_4$ grains and do not contribute to the change of resistivity.

Table A4 shows the atmosphere dependence of electric resistivity for undoped and 0.01 at.%Al-doped ZnO. As discussed above, there is no appreciable difference in resistivity between undoped and Al-doped ZnO. For both samples, the electric resistivity decreases by one or two orders of magnitude when heat-treated in vacuum and in argon compared with the case of heat treatment in air. It can be said that one of the reasons for the reduction of resistivity is the formation of oxygen vacancies, which causes the increase of conduction electron density. These observations support the interpretation given in Chapter 4 of PART I that oxygen vacancies would be formed at

grain boundaries in the local structures of ^{111}In–Al aggregations during heat treatment at a low partial pressure of atmospheric oxygen.

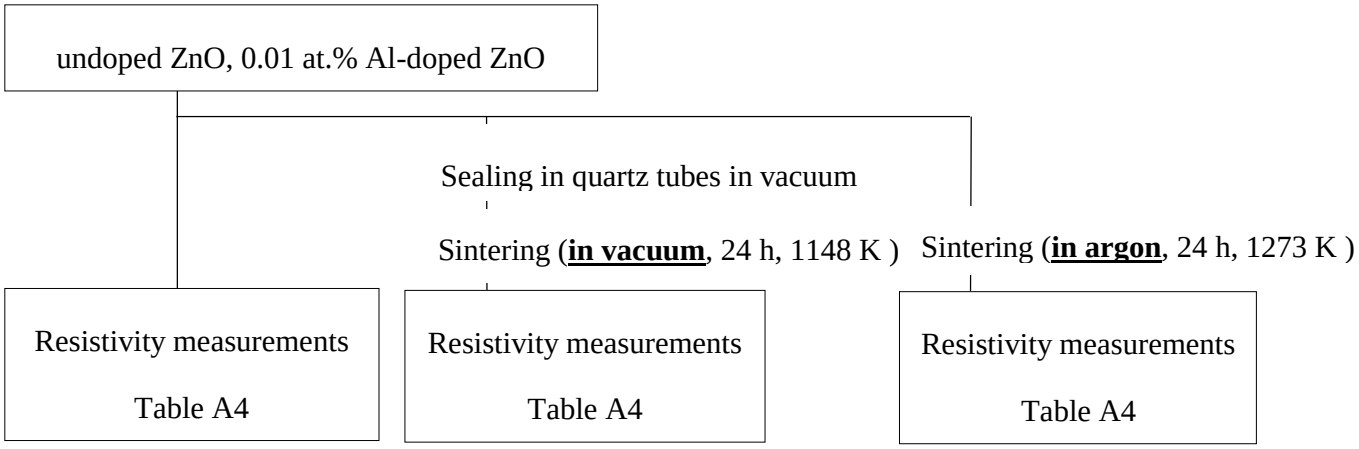

Fig. A8 Experimental procedure of sample preparation and resistivity measurements of undoped and 0.01 at.% Al-doped ZnO.

Table A3 Concentration dependence of electrical resistivity observed for Al-doped ZnO samples.

Al concentration (at.%)	Resistivity (Ω cm)
10	1.4×10^{4}
1	2.1×10^{4}
0.01	5.9×10^{3}
0 (undoped)	6.4×10^{3}

Table A4　Atmosphere dependence of electrical resistivity observed for undoped and 0.01 at.% Al-doped ZnO.

Annealing atmosphere	Resistivity (Ω cm)	
	undoped ZnO	Al-doped ZnO
in air	6.4×10^{3}	5.9×10^{3}
in vacuum	7.8	3.0×10^{2}
in argon	1.6×10^{2}	11

LIST OF PUBLICATIONS

Published Papers

[1] Sayaka Komatsuda, Wataru Sato, Satoshi Kawata, and Yoshitaka Ohkubo
"Strong Affinity between In and Al Impurities Doped in ZnO"
Journal of the Physical Society of Japan 80, 095001 (2011)

[2] Sayaka Komatsuda, Wataru Sato, and Yoshitaka Ohkubo
"Formation energy of oxygen vacancies in ZnO determined by investigating thermal behavior of Al and In impurities"
Journal of Applied Physics **116**, 183502 (2014)

[3] Sayaka Komatsuda, Wataru Sato, and Yoshitaka Ohkubo
"Thermal stability of locally-associated Al and In impurities in zinc oxide"
Journal of Radioanalytical and Nuclear Chemistry **303**, 1249 (2015)

[4] Wataru Sato, Yoshitaka Ohkubo, Yuki Itsuki, Sayaka Komatsuda, Daichi Minami, Toko Kubota, Satoshi Kawata, Akihiko Yokoyama, and Takashi Nakanishi
"Electric field gradient at the ^{111}Cd(←^{111}In) impurity sites in Ga-doped ZnO
Proceedings in Radiochimica Acta **1**, 435 (2011)

[5] Wataru Sato, Sayaka Komatsuda, and Yoshitaka Ohkubo
"Characteristic local association of In impurities dispersed in ZnO"
Physical Review B **86**, 235209 (2012)

[6] Wataru Sato, Sayaka Komatsuda, and Yoshitaka Ohkubo
"Characteristic interactions of ^{111}Cd probes with nonradioactive In impurities doped in ZnO"
Hyperfine Interactions **221**, 79 (2013)

[7] Wataru Sato, Rieko Mizuuci, Natsumi Irioka, Sayaka Komatsuda, Satoshi Kawata, Taoka Azuma, and Yoshitaka Ohkubo
"Extranuclear dynamics of ^{111}Ag(→^{111}Cd) doped in AgI nanoparticles"
Chemical Physics Letters **609**, 104 (2014)

[8] Wataru Sato, Sayaka Komatsuda, Yasuhiro Yamada, and Yoshitaka Ohkubo
"Detection of spinel $ZnIn_2O_4$ formed as nanostructures in ZnO"
Physical Review B **90**, 235204 (2014)

[9] Wataru Sato, Sayaka Komatsuda, Yasuhiro Yamada, and Yoshitaka Ohkubo
"Local structures at In impurity sites in ZnO probed by the TDPAC technique"
Journal of Radioanalytical and Nuclear Chemistry **303**, 1201 (2015)

[10] Wataru Sato, Sayaka Komatsuda, Rieko Mizuuci, Natsumi Irioka, Satoshi Kawata, and Yoshitaka Ohkubo
"Atomic-level observation of Ag-ion hopping motion in AgI"
Hyperfine Interactions, Published online (DOI 10.1007/s10751-014-1091-y)

Bulletins

[1] Sayaka Komatsuda, Wataru Sato, and Yoshitaka Ohkubo
"Observation of a Local Field at the ^{111}Cd(←^{111m}Cd) Probe in Al-Doped ZnO"
KURRI Progress Report **2010**, 94 (2011)

[2] Sayaka Komatsuda, Wataru Sato, and Yoshitaka Ohkubo
"Observation of a Local Field at the ^{111}Cd(←^{111m}Cd) Probe in Al-Doped ZnO",
KURRI Progress Report **2011**, 175 (2012)

[3] Sayaka Komatsuda, Wataru Sato, Satoshi Kawata, and Yoshitaka Ohkubo
''Interaction between PAC Probes and Aluminum Impurities Doped in Zinc Oxide''
Proceedings of the Specialist Research Meeting on "Condensed Matter Physics Research Using Short-Lived Nuclei and Radiations,
KURRI-KUR-168, 24 (2012)

[4] Sayaka Komatsuda, Wataru Sato, and Yoshitaka Ohkubo
"Local Association of Aluminum Impurities Doped in Zinc Oxide",
KURRI Progress Report **2012**, 113 (2013)

[5] Sayaka Komatsuda, Wataru Sato, and Yoshitaka Ohkubo
Proceedings of the Specialist Research Meeting on "Science and Engineering of Unstable Nuclei and Their Uses on Condensed Matter Physics'',
KURRI-KUR-177, 34 (2013)

[6] Sayaka Komatsuda, Wataru Sato, and Yoshitaka Ohkubo
"Dispersion State of Al and Cd Impurities in ZnO",
KURRI Progress Report **2013**, 103 (2014)

[7] Sayaka Komatsuda, Wataru Sato, and Yoshitaka Ohkubo
Proceedings of the Specialist Research Meeting on "Science and Engineering of Unstable Nuclei and Their Uses on Condensed Matter Physics'',
KURRI-KUR-195, 5 (2014)